NTNU

Norwegian University of
Science and Technology

Light Emission of Streamers in Dielectric Liquids

Jian Bin Ben Chen

Master of Science in Physics and Mathematics
Submission date: June 2017
Supervisor: Jon Andreas Støvneng, IFY
Co-supervisor: Lars Lundgaard, SINTEF Energy Research

Norwegian University of Science and Technology
Department of Physics

Abstract

Liquid insulation is widely used in various high voltage equipments crucial to a modern electrical grid. It is thus important to understand the behaviour and limits of performance for such liquids.

In these experiments, the emitted light from streamers in pure cyclohexane and pyrene dissolved in cyclohexane (0.06 M) were studied using photomultipliers, optical filters, an impulse generator and a point to plane electrode geometry with gap distance of ~ 4.0 mm. Needles with point radii of ~ 3 µm and ~ 15 µm were used as anodes, and were placed either in the bulk liquid or along a glass surface. The emitted ultraviolet light was studied qualitatively using a bandpass filter with peak transmittance at 200 nm, and the experimental results indicate that the fraction of emitted ultraviolet light increases with applied voltage before reaching a constant level in all experiments except when the needle electrode was placed along a glass surface, where the fraction increased without reaching a constant level. The streamers observed in these experiments had an average propagation speed that corresponds to second mode streamers, but extrapolation of the experimental results support the hypothesis of photoionization being a major propagation mechanism of higher mode streamers.

Furthermore, a strong light impulse, hereby named "onset flares" in this thesis, at the onset of streamer formation has been observed in preliminary studies. These high energy photons are believed to be an important feed forward mechanism for fast streamers with propagation velocity ~ 100 mm/µs. This phenomenon has otherwise not been reported.

The relation between the amplitude and delay time defined as the time from the applied negative impulse voltage reaching 90% of its minimum to the occurrence of an onset flare was studied. In some of the experiments, it was found that the amplitude decreased with

delay time. Space charge limited fields has been proposed as a possible cause for this observation.

Sammendrag

Væske-basert isolasjon er ofte brukt i forskjellige høyspenningskomponenter som er svært viktige i et moderne elektrisk nettverk. Det er derfor viktig å forstå oppførselen og begresningene for slike væsker.

I disse eksperimentene er det utsendte lyset fra streamere i ren sykloheksan og syklheksan med tilsatt pyreen (0.06 M) undersøkt ved bruk av fotomultiplikatorer, optiske filterer, en impulsegenerator og et punkt til plan elektrodegeometri med gapavstand ~ 4.0 mm. Nåler med punktradius ~ 3 µm og ~ 15 µm ble brukt som anoder, og ble enten plassert i testvæsken eller langs en glassoverflate. Det utsendte ultrafiolette lyset ble undersøkt kvalitativt ved å bruke et båndpassfilter med en maksimal transmittans ved 200 nm. De eksperimentelle resultatene indikerer at andelen av utsendt ultrafiolett lys øker med den påtrykte spenningen, før den når en konstant verdi i alle eksperimenter unntatt når nålen var plassert langs en glassoverflate, der denne andelen økte uten å nå en konstant verdi. Streamere observert i disse eksperimentene hadde gjennomsnittlige hastigheter som tilsvarer andre moders streamere, men ekstrapolering av de eksperimentelle resultatene støtter teorien om at fotoionisasjon er en viktig propagasjonsmekanisme for høyere moders streamere.

I tillegg har en sterk lyspuls, heretter kalt "onset flares" i denne avhandlingen, blitt observert i innledende forsøk. Disse høyenergifotonene kan være en viktig "feed forward"-mekanisme for raske streamere med propageringshastigheter på ~ 100 mm/µs. Dette fenomenet er ellers ikke blitt rapportert i tidligere studier.

Sammenhengen mellom amplituden og forsinkelsestiden definert som tiden fra den negative impulsspenningen når 90% av sitt minimum til en onset flare inntreffer er blitt undersøkt. I enkelte av eksperimentene ble det observert at amplituden minket med

forsinkelsestiden. Romladningsbegrensede felt har blitt foreslått som en mulig årsak til denne observasjonen.

Preface

This thesis was submitted to the Norwegian University of Science and Technology (NTNU) to fulfill my master's degree in applied physics.

This thesis was a part of a larger project at SINTEF Energy Research, where all the experimental work were performed with Lars Lundgaard as the main supervisor and Jon Andreas Støvneng as the internal supervisor. This thesis was also a continuation of my summer research internship at SINTEF Energy Research during summer 2016, and in a way a continuation of Jarl Øystein Samseth's master's thesis.

Acknowledgments

First of all, I would like to sincerely thank my main supervisor Lars Lundgaard and his colleagues Øystein Hestad, Dag Linhjell and Torstein Grav Aakre for their encouragement, support and expertise. A lot of issues were present after upgrading the equipment at the end of the summer internship, and still more problems regarding the equipments presented themselves after New Year 2017. In our desperate search after the roots of the problem, almost all electronic components in the setup were replaced before the problem was traced to a faulty resistor. In addition, I managed to accidentally melt the test cell after forgetting to fill it with liquid. However, my supervisors always remained calm and patient, and with their help and support, these issues were eventually resolved.

Secondly, I want to thank my friends Oda Lauten and Jan Gulla for giving me permission to base my LaTeX-template on the template that they made for writing the compendium of the subject TFY4155/FY1003 Electricity and Magnetism at NTNU. After all, not even a former chairman for the Compendium Committee and co-author can take whatever he wants.

Finally, I would like to wish my successor the best of luck. Oft as not, you may find yourself stuck with a technical problem, and start wondering if the actual objective of the experiment is to find (even more) supporting evidence of Murphy's law. In desperate days and sleepless nights, you may find comfort to think that, however small the contribution may be, your work will contribute to expand the horizon of scientific knowledge. Hence, I sincerely hope that you will be able to find courage and persistence to overcome your challenges and doubts.

Do your best today. Tomorrow you may perform even better.

Contents

CHAPTER 1

Introduction

Dielectric liquids are commonly used in electric devices such as capacitors, high voltage cables and transformers with the main purpose to prevent or rapidly suppress electric discharges. However, if the external electric field exceeds the liquid's dielectric strength, conducting plasma channels may be formed in the liquid, and dielectric breakdowns may occur. A dielectric breakdown can cause severe damage and/or degradation of the insulating material and the whole electric system.

Pre-breakdown phenomena in liquids mainly consist of propagating luminous plasma channels, and it is widely accepted to use the term "streamer" to describe all pre-breakdown phenomena in liquids observable through schlieren or shadowgraphic techniques [15]. However, even though the term "streamer" is directly adopted from gaseous discharges, streamers in liquids and streamers in gases refer to different phenomena, and unlike in gases, the physics of discharges in liquids are not well understood [19, 15]. The mean free path for the electron is crucial in modeling streamer propagation in gases. However, one of the fundamental differences and challenges is the higher density, which represents a shorter mean free path for the electron and fewer ionizing collisions. Thus, the same mechanisms used to model streamers in gases fails to describe streamers in liquids, and there are no predictive model for pre-breakdown phenomena in liquids. Therefore, streamers in liquids are mainly treated phenomenologically.

Traditionally, mineral oil has been widely used by the industry, but new vegetable esters, which are much more environmentally friendly, are gradually taking over. However,

breakdown and the most severe fast streamers typically occur at a lower voltage for most of these esters, at a lower voltage. In order to improve the performance of these esters, it is necessary to improve the understanding of the physics behind the processes that lead to breakdown.

The main purpose of this master's thesis is to study the light emitted by the streamers qualitatively using photomultipliers and a point to plane electrode geometry to clarify if and how emitted high energetic light may contribute to support propagation via a process known as photoionization. The experiments were mainly conducted in cyclohexane with a purity of 99.9% and cyclohexane with dissolved pyrene (0.06 M). As outlined in 2.2.2, calculations have shown that light in the UV domain are most relevant for photoionization in cyclohexane. However, photons with the relevant energies may be frequently absorbed by cyclohexane molecules, and are thus hard to detect. Experiments were therefore performed both with the needle electrode placed in the bulk liquid and along a glass surface in order to allow streamers to propagate along the glass surface, and thus reduce the amount of light absorbed by the test liquid.

In addition, preliminary studies have registered strong light impulses at high voltages at the start of streamer formation, which has not been reported in previous studies, and may be an important feed forward mechanism for high mode streamers. The second purpose of these experiments is to further investigate mechanisms that may contribute to the initiaion of such light signals by studying the relation between delay time[1] and amplitude.

This master's thesis is a continuation of my specialization project completed at NTNU in Autumn 2016, which had an almost identical objective and used a similar experimental setup. Thus, chapter 1, 2 and 3 are partly based on [4].

[1] See 2.3.

CHAPTER 2

Theory

This chapter gives a short introduction to relevant concepts of streamers. A short introduction on streamer classification is given in section 2.1, while section 2.2 considers propagation mechanisms and gives short outlines of photoionization, impact ionization and field ionization. Lastly, section 2.3 describes a newly discovered phenomenon where short powerful light signals were observed at what seems to be streamer inception.

2.1 Streamers

A streamer consists of a propagating ionizing front called streamer head and a plasma-filled tail in the wake of the streamer head called a streamer channel. The polarity of the streamer head is equal to the polarity of the electrode that the streamer extends from. See figure 2.5 for a simplified illustration. The voltage required to initiate a streamer is called the initiation voltage.

The insulating properties of a material is traditionally characterized by its dielectric strength, which is the critical magnitude of the applied electric field at which the insulating ability of the material fails. This is often also given as the breakdown voltage V_b, which is the voltage that gives a 50% probability of electrical breakdown. In the case of streamers, the breakdown voltage can be regarded as the critical voltage required for the streamer to bridge the gap between the electrodes and thereby cause an electric break-

down. At voltages between the initiation voltage and breakdown voltage, the streamer will propagate a distance in the gap between the electrodes before it stops and extinguishes. This is due to the reduced field at the streamer head that is caused by voltage drop along the streamer channel or branching of the channels such that it is no longer able to ionize the liquid. The distance is called the stop length, and it has been observed that it increases with voltage and can be reduced by increasing the pressure [13].

Compared to negative streamers, positive streamers have a lower breakdown voltage. Thus, positive streamers are generally considered more dangerous for electrical equipments, and most research are therefore focused on positive streamers. In this thesis only positive streamers are studied.

2.1.1 Classification

Streamers are classified into different modes based on their propagation velocity, an idea that was first proposed by Hebner [14]. The propagation velocity of each mode typically differs by a factor of 10. Streamers in the first mode propagate with velocities on the order of 0.1 mm/µs, second mode streamers propagate at 1 mm/µs etc. Pictures of streamers in various modes are shown in figure 2.1, and a plot of the average streamer propagation speed V.S. applied voltage is presented in figure 2.2.

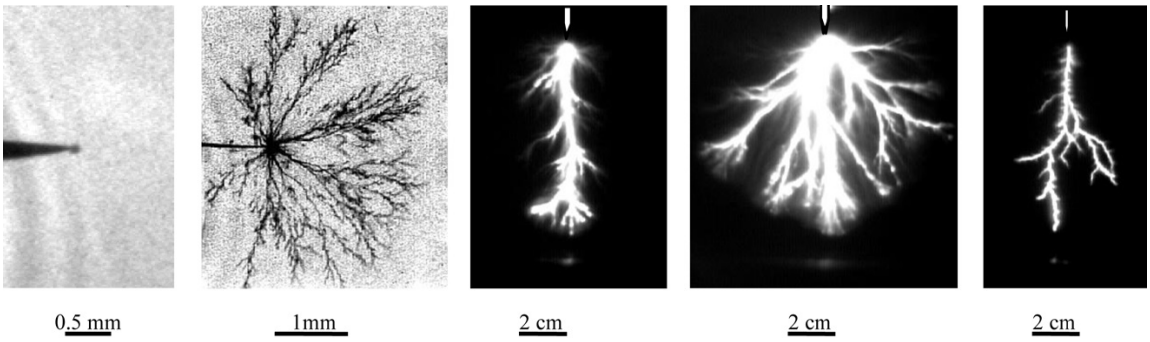

Figure 2.1: Pictures of positive streamers in transformer oil. From left to right: 1st mode, 2nd mode, 2nd mode, 3rd+2nd modes and 4th mode. These pictures are taken from [19].

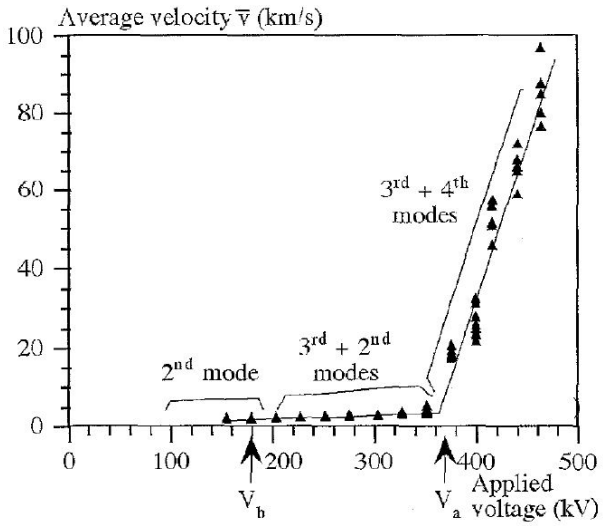

Figure 2.2: Average streamer propagation speed V.S. applied voltage in a 10 cm gap for streamers in transformer oil. This figure is taken from [23].

First mode streamers are bush-like, and will normally not cause a breakdown because it will only propagate a small distance before the electric field at the streamer head fails to ionize the liquid in front of it.

If the voltage is higher, but below the breakdown voltage, second mode streamers can be initiated. Second mode streamers have a filamentary appearance, and its speed only weakly depends on the applied voltage, while the number of filaments increases significantly with applied voltage [23]. Since second mode streamers dominate up to the breakdown voltage, they are considered of great importance as they are an important factor in determining the breakdown voltage.

At voltages above the breakdown voltage and below the acceleration voltage V_a, which is the voltage that causes the transition of third mode streamers to fourth mode streamers, third mode streamers can be initiated. At the mentioned voltages, the third mode streamers typically propagate a distance into the medium before switching to second mode. Above the acceleration voltage, instead of slowing down to the second mode, the third mode switches to the fourth mode as mentioned. Fourth mode streamers are difficult to characterize due to its high propagation speed. The propagation speed has been estimated to be above 100 mm/µs, and it has been observed that it consists of only 1-2 very luminous branches with a few lateral branches [23].

It has been observed that third mode streamers propagating in water generate succes-

sive spherical shock waves [2] as seen in figure 2.3. This observation indicates stepped propagation with high frequency short steps.

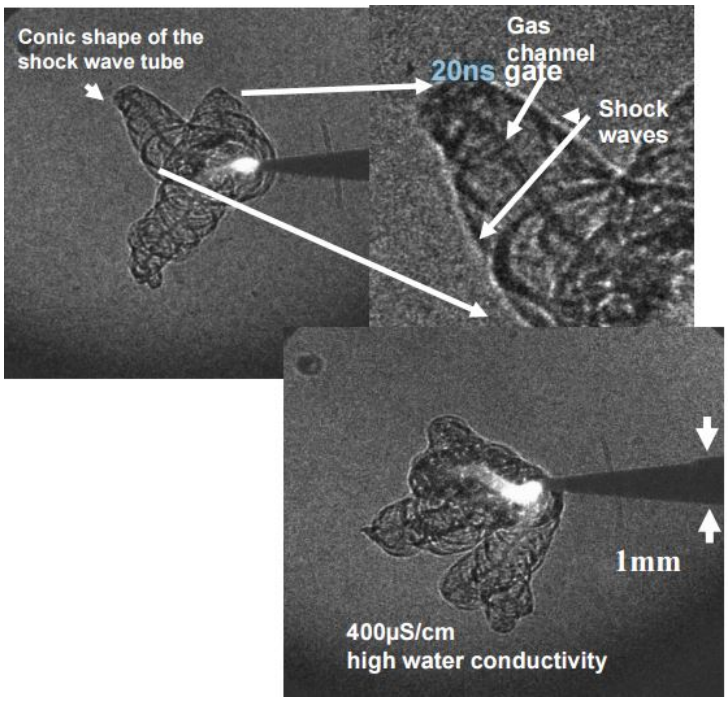

Figure 2.3: Plasma channels propagating in water give rise to discrete shock circles. The distance between two circles is of tens of µm. These pictures are taken from [2].

2.1.2 Streamer along an Insulating Surface

A pressboard placed parallel to the electric field has been observed to enhance the propagation of streamers in mineral oil [22]. Lesaint and Massala hypothesized that the streamer channels distort and reduce the electric field of each other, a phenomenon known as shielding. This phenomenon is illustrated in figure 2.4, which shows streamers extending from needle electrodes, and one of them are placed along an insulating surface. When the electrode is placed along an insulating surface, the number of streamer branches are reduced, so that the shielding effect should also be reduced.

Lesaint and Masala also proposed that this shielding effect is reduced significantly once the applied voltage reaches the acceleration voltage because of a significant reduction of the number of branches. Streamers propagating along an insulating surface (or in bulk liquid) therefore propagates slowly between V_b and V_a, and undergoes a rapid change in propagation velocity once the applied voltage reaches V_a.

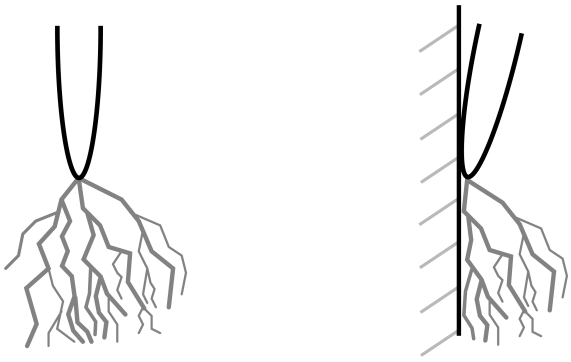

Figure 2.4: Streamers extending from needle electrodes. The streamers extending from the electrode to the left can propagate freely, while streamers extending from the electrode to the right are constrained by an insulating surface.

Thus, if the electrode is placed along an insulator so that the streamers propagate along an insulating surface, roughly half of the shielding effect would be removed. V_a should therefore be reduced.

Moreover, electrons that collide with a dielectric surface can either be absorbed by the surface and give it a negative charge, or cause the emission of additional electrons in a process known as secondary electron emission [16]. If the energy of the incident electron is below a certain threshold, absorption will dominate and thus deprive a streamer of free charges.

Another way a dielectric surface may affect streamer propagation is through absorption of the photons emitted by the streamers. A photon that hits the surface may excite a molecule, which will eventually return to its ground state through various energy loss mechanisms. One of the possibilities is re-radiating a photon, but de-excitation via non-radiative processes such as molecular disassociation or vibration tend to be more likely to dominate. For radiation to dominate, it must be faster than the non-radiative processes, which is usually not the case. Typical time for radiative de-excitaiton is $10^{-9}\,\mathrm{s}$, while it is $10^{-13}\,\mathrm{s}$ for vibrational de-excitation[16]. Hence, most molecules absorb photons, but do not re-emit them. Furthermore, photons re-radiated by an excited molecule usually have far less energy than the absorbed photon [5].

Lastly, a dielectric surface will also alter the electric field. For an isotropic material, the electric displacement field $\mathbf{D}$ is proportional to the electric field:

$$\mathbf{D} = \varepsilon_0 \varepsilon_\mathrm{r} \mathbf{E} = \varepsilon \mathbf{E}, \tag{2.1}$$

where ε_r is the relative permittivity and ε is the permittivity of the material. From Gauss' law

$$\oiint_A \mathbf{D} \cdot \mathrm{d}\mathbf{A} = Q_\mathrm{f}, \tag{2.2}$$

where Q_f is the free charge, we can obtain the boundary condition for the component of $\mathbf{E}$ orthogonal to the boundary of a dielectric interface with permittivities ε_1 and ε_2. This is given by

$$\varepsilon_1 E_{1\perp} - \varepsilon_2 E_{2\perp} = \sigma_\mathrm{f}, \tag{2.3}$$

where σ_f is the free surface charge density.

The component of $\mathbf{E}$ parallel to the interface is however continuous across the boundary, but the fact that the orthogonal component is discontinuous will will lead to a distorted field that is dependent on ε_1, ε_2 and σ_f.

2.2 Streamer Propagation and Ionization Mechanisms

Studies have shown that inception of both first and second mode may be caused by the same process [12]. The first discharge in the liquid can cause a shock wave to propagate outward from the electrode [15], which will in turn create an ionized bubble. If the applied voltage is above a certain limit called the propagation voltage V_p, second mode streamers will start to propagate [15]. The electric field at the bubble's boundary is now strong enough to ionize the liquid-bubble interface through electron avalanches or direct field ionization if the field strength is sufficiently large [15]. A propagating ionizing region is thus created, and it will leave a trail of conducting plasma behind, which will connect it to the electrode it extended from. A simplified outline for the propagation of a positive second mode streamer is given in figure 2.5.

In gaseous breakdowns, a process known as the Townsend mechanism is known to be important [25]. The first step of a positive Townsend discharge is the creation of a seed electron in the proximity of the anode. The electric field will then accelerate the seed electron towards the anode, and thus increase the kinetic energy of the electron until it collides with another atom/molecule. If the mean free path is sufficiently large, the electrons will gain enough energy between collisions to either ionize the atom/molecule, or transfer part of its energy to excite the atom/molecule. If a collision between the electron

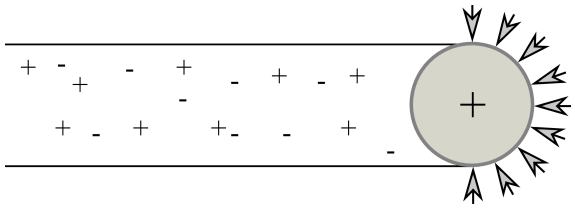

Figure 2.5: A simplified illustration for the propagation of a positive second mode streamer. The propagating ionizing front called a "streamer head" (grey region) leaves behind a trail of conducting plasma, and can thus be considered as an extension of the electrode it originated from. The electric field at the boundary of the streamer head combined with the applied electric field is strong enough to ionize the liquid in front of it through electron avalanches represented by the arrows. If the electric field has sufficient strength, direct field ionization is also possible.

and the atom/molecule X yields n additional electrons, this process can be written as

$$X + e^- \rightarrow X^{n+} + (n+1)e^-.$$

This will result in a chain reaction called an electron avalanche that generates a large amount of free electrons. The ions that are left behind will remain more or less stationary and constitute an extension of the streamer's electric potential. This will lead to new electron avalanches and the growth of the streamer.

However, despite the success in describing gaseous discharges, the density in liquids is too high for the Townsend mechanism to explain the observed breakdown voltages[1]. Low density regions, which is believed to be important for inception of positive first mode streamers [15], can however be formed by mechanisms such as joule heating [1], electromechanical forces [24], and Coulomb repulsion between local homocharges [32].

Ionization mechanisms can be grouped into the three main categories impact ionization, photoionization, and field ionization. These are all used to explain the various conductivity and streamer propagation mechanisms, and are believed to dominate at different streamer modes. Photoionization is for instance believed to dominate for fast events like fourth mode streamers, but studies suggest that it may also be important for second and third mode streamers [26].

[1]The Townsend mechanism's dependence on the density is shown in appendix A

2.2.1 Impact Ionization

Impact ionization is the most important mechanism in Townsend discharges, and even though Townsend discharges are not able to describe streamers in liquid in a satisfactory way, impact ionization is still considered as an important mechanism in the dense gas approximation, where the liquid is described as a semi conductor [3].

This ionization mechanism is caused by the transfer of the kinetic energy in a collision between an electron and an atom/molecule. For an electron with mass m_e moving with speed v_1 colliding into an atom/molecule with mass M[2] moving with speed v_2, this exchange of energy can be written as

$$\frac{1}{2}m_e v_1^2 + \frac{1}{2}M v_2^2 = \frac{1}{2}m_e v_1'^2 + \frac{1}{2}M v_2'^2 + \Delta E_\mathrm{k}, \tag{2.4}$$

where v_1' and v_2' are the the speed of the electron and the atom/molecule after the collision, respectively.

For an elastic collision, the change in kinetic energy ΔE_k is equal to zero. Since the atom/molecule has a much larger mass than the electron, this process can be considered as the electron scattering off the atom/molecule, which remains approximately at rest. Thus, neither the energy of the electron nor of the atom/molecule are changed.

In the case of an inelastic collision, however, the electron transfers part of its energy to the atom molecule. This energy may excite electrons in the atom/molecule, excite molecular vibrations or ionize the atom/molecule.

For an impact ionization to occur, the incoming electron have to possess energy higher than the ionization potential V_i, which is the amount of energy required to remove a valence electron from an atom[3], of the atom/molecule. If the ionization potential is high compared to the average energy of the electrons, the probability for a successful impact ionization can be modeled as being proportional to the number of electrons with energy above the ionization potential [31], which is given by

$$N_e = \int_{V_\mathrm{i}}^{\infty} f_e(\varepsilon)\,\mathrm{d}\varepsilon, \tag{2.5}$$

[2] Assuming that the change of mass of the atom/molecule after the ionizing collision is negligible.
[3] Commonly denoted as IP.

where $f_e(\varepsilon)$ is the energy distribution of the electrons, with a field dependence that is in general unknown.

For sufficiently strong electric field and/or sufficiently long mean free path length, the electrons can ionize one or more atoms/molecules before being absorbed. This will result in an electron avalanche where the initial seed electron is effectively multiplied into a large number of electrons. Due to the high density, and thus low mean free path length, electron avalanches in liquids are generally considered a controversial topic. Nevertheless, experiements conducted with negative polarity in cyclohexane under impulse and DC voltage suggest that the onset of streamers in the liquid is caused by an electron avalanche in the liquid phase [9, 10].

2.2.2 Photoionization

For the transition from second to higher modes, ionization by electron impact alone is unable to ionize the liquid in front of the streamer head fast enough to explain the propagation velocity of the streamers [27]. Photoionization has thus been proposed as an important process that enhances the propagation of the higher mode streamer.

Calculations have shown that the ionization potential V_i decreases rapidly when E increases [7]. Furthermore, when E is above a critical value E_c [4], the excited states of the molecule vanishes. What is left is a two-state system consisting only of the ground state and the ionized state as illustrated in figure 2.6.

As mentioned previously, an electron avalanche may leave the some of the atoms and molecules in an excited state. When these atoms and molecules de-excite, photons with energy E_γ are emitted. If E_γ is larger than V_i of the atoms/molecules, then the photons are able to ionize the atoms/molecules close to the streamer head and thereby liberate more electrons. As $E \to E_\mathrm{c}$, the number of possible excited states decreases. Thus, it becomes more and more likely that the excited atoms and molecules emit photons with higher energy when they de-excite. Furthermore, since V_i is reduced by the external field, the atoms/molecules in a high field region become easier to ionize. This is an efficient way of moving the high field region with a large density of ions, that may explain the transition from second to higher modes [27].

[4] Dependent on the type of molecule.

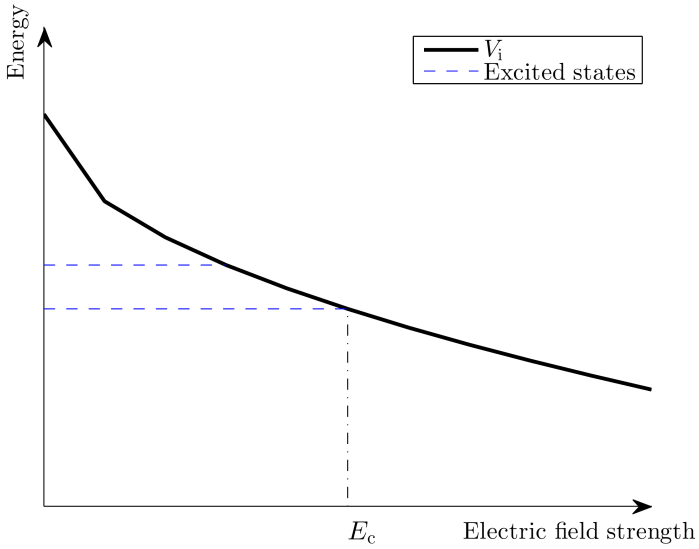

Figure 2.6: Simple illustration of how the excited states of a molecule may vanish when the external electric field strength exceeds a critical value E_c. Above this value, the molecule is a two-state system consisting only of the ground state and the ionized state.

The ionization process involving a photon γ and an atom/melocule X can be written as

$$\gamma + X \rightarrow X^+ + e^-.$$

These electrons can then act as new seed electrons for new avalanches close to the streamer head and thus create a propagating ionizing front with high propagation velocity.

In appendix A it is shown that the kinetic energy of electrons is proportional to the applied electric field strength E. Increasing the applied voltage V, and thereby E, should therefore also increase E_γ and the amount of photons emitted by the streamers. Fast streamers are therefore expected to be observed more often as the voltage is increased.

Constrained density functional theory has been used by Davari et al. to calculate the excited states for different molecules, amongst them cyclohexane [8]. First excited state for cyclohexane is 7 eV above ground state. Thus, in order for a photon to excite a cyclohexane molecule from ground state to the first excited state in one step, a photon with wavelength 178 nm or shorter is required.

The calculated ionization potential for pyrene is 7.11 eV [7].

2.2.3 Field Ionization

Field ionization is a mechanism that is dependent on tunneling [30]. Normally, the probability for tunneling is low in neutral atoms, but the potential barrier is lowered if the atom is placed in an external electric field, which facilitates tunneling.

For barrier heights dependent on the external electric field, the tunneling time τ for an electron with energy ε_i in the state i described by the wavefunction ψ_i is given by [28]

$$\tau \propto \frac{\psi_i(R_-)}{\psi_i(R_+)}, \tag{2.6}$$

where $R_\pm$ are the classical turning points where the electron energy ε_i is equal to the potential, I.e. when $V(R_\pm) = \varepsilon_i$. For a small external electric field $E \ll \varepsilon_i$ [5], the classical turning points in atomic units are given by

$$R_+ = -\frac{1}{\varepsilon_i} \tag{2.7}$$

$$R_- = -\frac{\varepsilon_i}{E} - \frac{1}{\varepsilon_i}, \tag{2.8}$$

and the tunneling time may be calculated using the WKB approximation.

2.3 Onset Flare

In preliminary studies, powerful signals lasting a few nanoseconds at what seems to be streamer inception has been observed at voltage level $\gtrsim 40\,\mathrm{kV}$ in pure cyclohexane. An example of such a signal can be seen in 2.7, which shows part of a signal registered by a photomultiplier. These high energy photons may be crucial for the feed forward mechanism of the fast streamers ($\sim 100\,\mathrm{mm/\mu s}$).

Measurements performed during the specialization project failed to find any correlation between the amplitude of the onset flares and the applied impulse voltage [4]. The measurements in this thesis will focus on examining the correlation between the amplitude and the delay time t_D), which is defined as the time between the voltage impulse reaching 90% of minimum and the onset flare reaching its minimum.

[5] Atomic units.

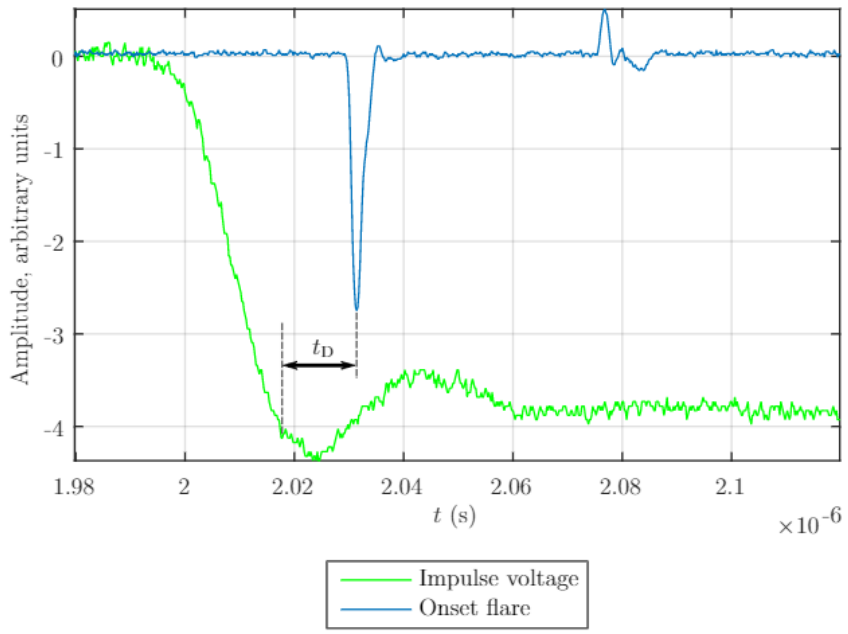

Figure 2.7: A typical scaled multiplot of the measured signals where the voltage is measured as a function of time. Shortly after the impulse voltage has reached minimum, both photomultipliers registered a powerful signal. The measurement was performed in pure cyclohexane at 50 kV without any optical filter. t_D is the time between the voltage impulse reaching 90% of minimum and the onset flare reaching its minimum.

CHAPTER 3

Experimental Setup and Procedure

This chapter is divided into two parts. The first section describes the experimental setup with its various components and gives a short introduction to relevant concepts of photomultipliers. In addition, a short description of the test liquids is also given.

The second section shortly outlines the measurement process and the methods that were used to analyze the data.

3.1 Setup

The setup mainly consisted of an impulse voltage generator, a test cell, an optical filter, two lenses and two photomultipliers (PM) as shown in figure 3.1. The voltage over the test cell is generated by an impulse generator with rise time $\sim 20\,\text{ns}$, that may initiate streamers in the test cell. The light emitted by the streamers inside the test cell would then be focused by the lenses[1] and measured by the photomultipliers to the left and right of the test cell, which are placed a distance from the image plane in order to avoid overstressing the instruments. After passing through the lenses, light propagating towards PM2 also has to pass through an optics tube that may contain an optical filter, while light propagating towards PM1 reached it directly after passing the lens. These two signals from the photomultipliers and the probed impulse voltage were recorded by an

[1] Transparent in the UV region.

oscilloscope with maximum sampling rate 5 GS/s[2].

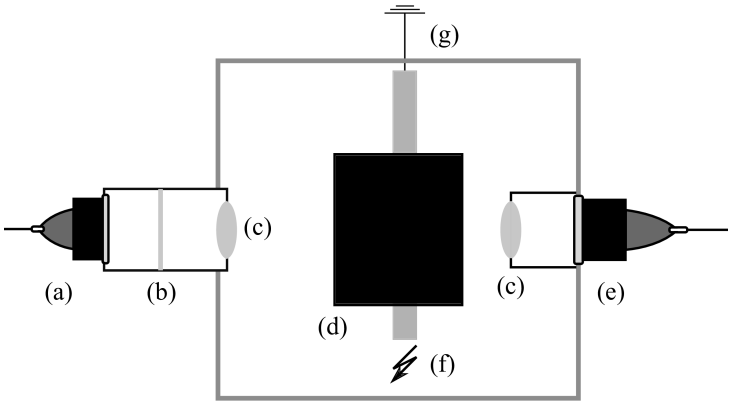

Figure 3.1: A simplified outline of the experimental setup. (a) PM2, (b) an optical filter may be placed here, (c) lenses transparent in the UV region, (d) test cell, (e) PM1, (f) impulse voltage from the impulse generator, (g) grounded metal box sealed to avoid external light.

The signals from the photomultipliers could then be compared in order to study the amount of light emitted at different regimes (inserting a UV-filter and comparing the signals from PM1 and PM2 would for instance provide information about the amount of light emitted in the UV region). However, this method can only give a rough idea about the intensity at various frequencies, but the main interest of this thesis is to only qualitatively compare the amount of emitted UV light against other frequencies.

The test cell was placed inside a grounded metal box, and both the box and the optics tube are sealed to avoid external light. Furthermore, it was also possible to clean the test liquid after applying a voltage impulse by connecting the test cell to a liquid circulation system consisting of a pump and filters. This was only done in experiments involving pure cyclohexane because of health and security issues associated with pyrene.

3.1.1 Electrode Geometry

Electrode configurations like plane-plane, sphere-sphere and needle-plane are commonly used in streamer-related research. The ideal plane-plane configuration gives rise to a uniform electric field between the plane electrodes, the sphere-sphere configuration has a divergent symmetric field between the spheres, while the electric field between a needle-plane configuration is divergent and asymmetric.

[2]Tektronix DPO4104

The needle-plane configuration has been chosen because the strong divergent field at the needle electrode enables the generation of a strong electric field at a much lower voltage compared to for instance the plane-plane configuration. Furthermore, the use of a needle-plane configuration also simplifies the study of streamers along a dielectric surface since the initiation of streamers is located, and it is far easier to place a needle electrode along a surface than to for instance place a spherical electrode along a plane surface.

Methods of applying electric power to these configurations include gradual incrementation of DC or AC voltage, lightning impulse, and step voltage. The latter has a voltage-time curve that rises from zero to a (ideally) constant maximum voltage in a matter of nanoseconds, and is the preferred choice for studying breakdown mechanisms, as it gives a much better control of the voltage. The first two methods are commonly used to benchmark electrical equipments and insulating materials.

The electric field in a needle-plane geometry is calculated using the hyperbolic approximation, where the needle-plane configuration is modelled as a rotationally symmetric hyperboloid with tip curvature r_p placed at a distance d above an infinite plane. In this configuration, it is possible to solve the Laplace equation for the electric field analytically in prolate spheroid coordinates.

For $r_\mathrm{p} \ll d$, the electric field along the axis of rotation of the hyperboloid can be written as [6]

$$E(x) = \frac{2Vd}{(2xd + r_\mathrm{p}d - x^2)\ln(4d/r_\mathrm{p})}, \tag{3.1}$$

where V is the potential of the needle tip.

The electric field is strongest at the needle tip, and is given by

$$E_\mathrm{p} = E(0) = \frac{2V}{r_\mathrm{p}\ln(4d/r_\mathrm{p})}. \tag{3.2}$$

In a dielectric, the conductivity typically increases exponentially with the electric field. This increase in conductivity in the high field regions will cause charge separation and charge buildups that impose a limit on the electric field. The resulting field is called a space charge limited field (SCLF) [15].

In the SCLF region, the field is essentially determined by the space charge, and is almost constant [15]. In this region, the field can be significantly lower than the Laplacian

field like in equation (3.1), but on the other hand, the volume of the high field region is increased by the space charge. This is qualitatively illustrated in figure 3.2, where a SCLF at times $t_1 < t_2 < t_3$ is plotted together with a Laplacian field. As time increases, the strength of the high field region is reduced, but the volume of the high field region is increased. All fields in figure 3.2 are axial fields along the symmetry axis from the apex of a semi-spheroid.

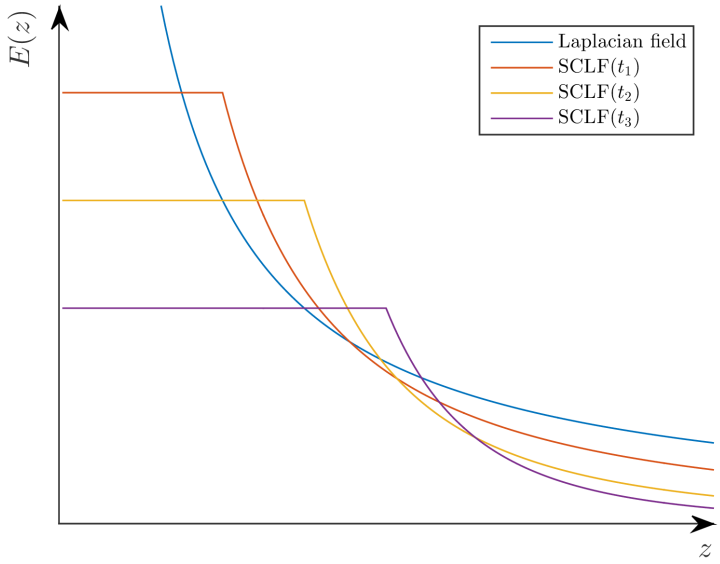

Figure 3.2: An illustrastion of a SCLF at times $t_1 < t_2 < t_3$, which is plotted together with a Laplacian field. As time increases, the strength of the high field region is reduced, but the volume of the high field region is increased. All fields are axial fields along the axis from the apex of a semi-spheroid.

3.1.2 Photomultipliers

The photomultipliers used in the experiments are Hamamatsu R2286U-02 (PM1) and PHOTEK PMT310 (PM2). The risetime of PHOTEK PMT310 is 120 ps, and was used to give a qualitative picture of the amount of emitted light at various wavelengths by using various optical filters. Hamamatsu R2286U-02 has a risetime of 336 ps, and was used to generate a reference signal.

Both photomultipliers are microchannel plate photomultipliers. A simple outline of such a photomultiplier is shown in figure 3.3. A photon incident on the photocathode may cause the photocathode to emit an electron due to the photoelectric effect if it possesses

sufficient energy. This photoelectron will then be accelerated towards a microchannel, where it will repeatedly collide against the walls. The impacts will cause the walls in the microchannel to emit secondary electrons in a process known as secondary emission of electrons, which will result in a cascade of electrons all propagating towards the anode. The current through the anode can then be measured.

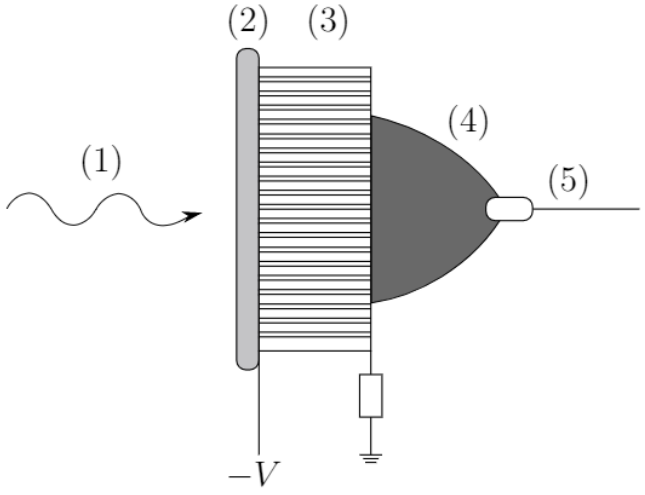

Figure 3.3: Simple outline of a microchannel plate photomultiplier. (1) Incident photon, (2) photocathode, (3) microchannel plate, (4) anode, (5) output signal.

Not every photon hitting the photocathode will result in emitted photoelectrons even if the energy of the photon is above the band gap of the photocathode material. The emission of photoelectrons has a stochastic nature that depends on the energy of the photon, since a photon with large energy has a higher probability of lifting an electron from the valence band to the conduction band. This can be characterized by the quantum effciency η_{q}, which is the ratio of the number of emitted photoelectrons to the number of incident photoelectrons. For a photon with wavelength λ, this is given by

$$\eta_{\mathrm{q}} = S(\lambda)\frac{hc}{\lambda}, \tag{3.3}$$

where h is Planck's constant, c is the speed of light in vacuum and $S(\lambda)$ is the cathode radiant sensitivity defined as the ratio of photoelectric current to incident radiant flux at wavelength λ.

Thus, if the incident radiant flux is low, it will be impossible to distinguish between pulsed and continuous light. This issue may be further complicated by dark currents, which is a current in photosensitive devices in the absence of external radiation. Dark currents are caused by the random generation of charges due to thermal fluctuations, and

is thus temperature dependent. Box plots of the amplitude of the dark currents of both photomultipliers as function of the photomultiplier voltage are shown in figure 3.4 and 3.5.

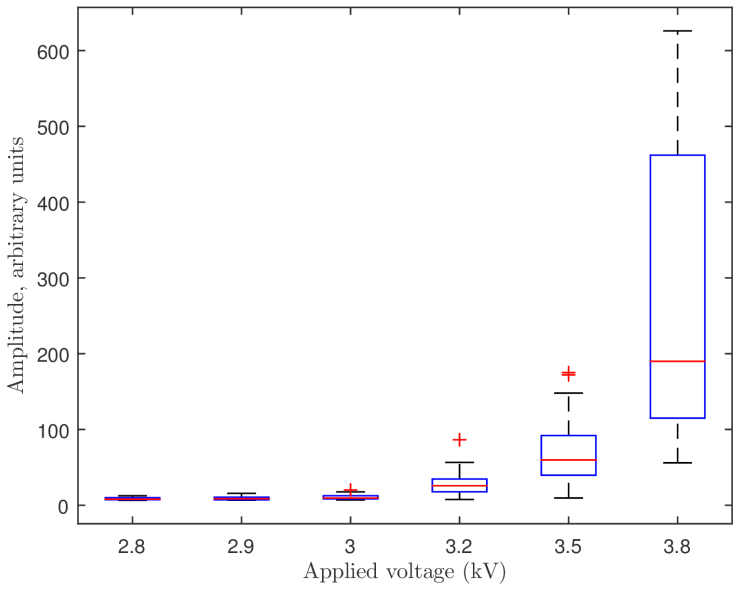

Figure 3.4: A box plot of the amplitude of the dark current as function of applied photomultiplier voltage for Hamamatsu R2286U-02 (PM1).

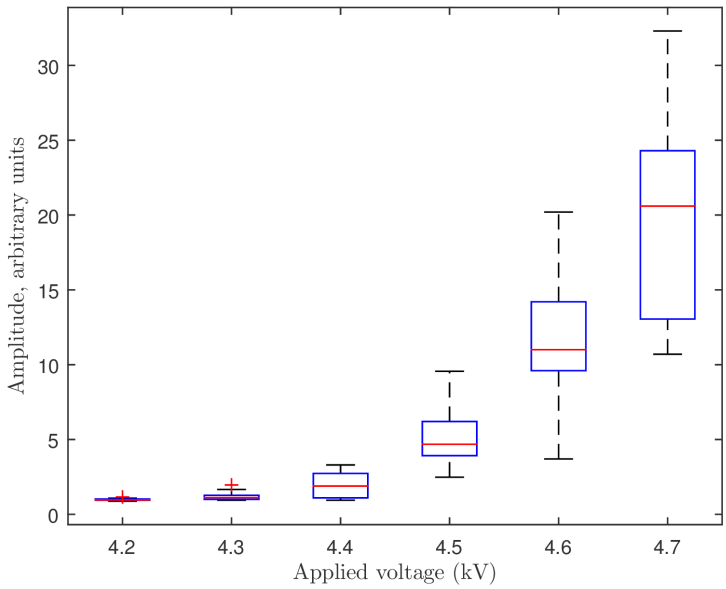

Figure 3.5: A box plot of the amplitude of the dark current as function of applied photomultiplier voltage for PHOTEK PMT310 (PM2).

3.1.3 Test Cell

The test cell has a cylindrical structure, and is illustrated in figure 3.6. The test liquid is contained between two glass windows of fused quartz silica with relative permittivity 3.8 and thickness 4 mm, which are also transparent in the UV region.

The electrodes were separated by a distance d between 3.5 mm and 4 mm. For the anode, needles with point radii r_p of $\sim 2\,\mu$m and $\sim 15\,\mu$m were used. The cathode has a semi-cylindrical form to fill the lower part of the test cell, and the flat part facing the anode has dimension 35 mm $\times$ 29.4 mm. The anode was grounded, and negative high voltage pulses at the cathode were supplied by the impulse generator. The needle electrodes could either be placed along one of the windows or in the bulk liquid, but past experiments showed that this will damage the window. One of the windows were therefore reinforced with two glass plates for the experiments where the needle electrode was placed along the glass surface.

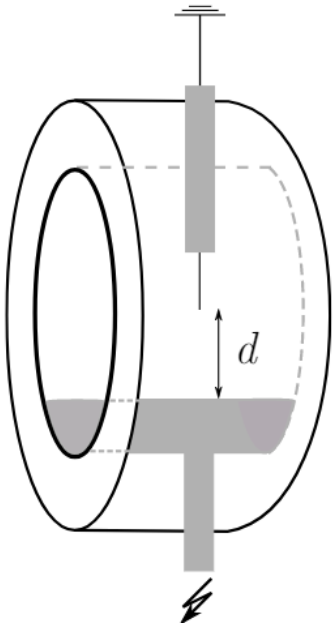

Figure 3.6: Sketch of the test cell containing the electrodes with a separation distance d and the test liquid between two glass windows of fused quartz silica.

3.1.4 Optical Filters

Two optical filters were used in these experiments. One UV bandpass filter with peak transmittance at 200 nm, and one longpass filter that is transparent for most of the visible light. The cut-off for the longpass filter is at 280 nm.

3.1.5 Test Liquid

Cyclohexane (C_6H_{12}) was chosen because it is a common liquid used in streamer experiments to model complex mineral oils. In order to relate the observed photons to the molecular structure, knowledge about the excited states, ionization potential and the field dependence of these are required. As already mentioned in 2.2.2, these have been calculated for cyclohexane.

In addition, cyclohexane is easy to obtain in spectroscopic grade, and is a good solvent, which makes it easy to add additives in order to look at how molecules with specific properties like low ionization potential may influence the results. The cyclohexane used in the experiments is of spectroscopic grade with a purity of 99.9%.

Pyrene[3] was chosen as the additive for the experiments. At room temperature, 1 L of cyclohexane is saturated when 19 g of solid pyrene is dissolved, which corresponds to a pyrene concentration of 0.1 M. To avoid over-saturation, a concentration of 0.06 M was chosen.

This additive will decrease the breakdown voltage and enhance the branching of streamers [21]. Thus, streamers propagating in a liquid cyclohexane with pyrene additives tends to be much more filamented, and a large increase of the acceleration voltage has been observed [21]. This can be explained by the the shielding effect, since the tip field of the streamers are decreased when more streamer filaments propagate together and shield each other.

3.2 Methods and Procedures

3.2.1 Measurement Process

A LabVIEW procedure was used to trigger the impulse voltage generator, and record the data from the oscilloscope. Impulse voltages ranging from 20 kV to 70 kV were applied over the plane-needle gap.

[3] A polycyclic aromatic hydrocarbon with chemical formula $C_{16}H_{10}$.

Eight voltage impulses were applied for each voltage level. After each voltage impulse, the LabVIEW procedure recorded the data from the oscilloscope, which included the signals from the two photomulitipliers and the probed voltage. For experiments using pure cyclohexane as a test liquid, the test liquid was circulated and filtered for three minutes. After filtering, the pump was stopped for another three minutes to allow the liquid to come to rest before the impulse voltage generator was triggered again. For experiments involving pyrene additives, the filtering process was skipped.

After these eight voltage pulses at the same level, the voltage was increased by 5 kV until the defined maximum voltage is reached. The measurement series is then finished for one configuration of the setup.

The damaged glass, needle electrode and the test liquid was then replaced with unused samples, the test cell cleaned and the experiment was repeated for other parameters. The parameters that can be changed between the experiments are summarized in table 3.1.

Parameter	Configuration 1	Configuration 2
Needle position	In the bulk liquid	Along glass surface.
Needle point radius r_p	3 µm	15 µm
Test liquid	Pure cyclohexane	0.06 M Pyrene in cyclohexane

Table 3.1: The varied parameters in addition to the voltage impulses. The needle was either placed inside the bulk liquid or along the surface of one of the windows of the test cell, and needles with two different point radii were used. Most experiments were performed in pyrene dissolved in cyclohexane with a concentration of 0.06 M, but pure cyclohexane was also used.

3.2.2 Data Analysis

Detected light is represented on the oscilloscope screen as "spikes", i.e. sharp local minima extruding from a background voltage signal measured as a function of time. A typical plot of the measured signals is shown in figure 3.7.

The recorded data was analyzed using a self-written MATLAB script whose main purpose was to count the spikes from both PM1 and PM2 and compare these numbers.

The background signal was always fluctuating with a small, almost constant amplitude around an equilibrium. Therefore, in order to count the relevant spikes, a limit had to be defined depending on the voltage level and the configuration of the setup. This limit was

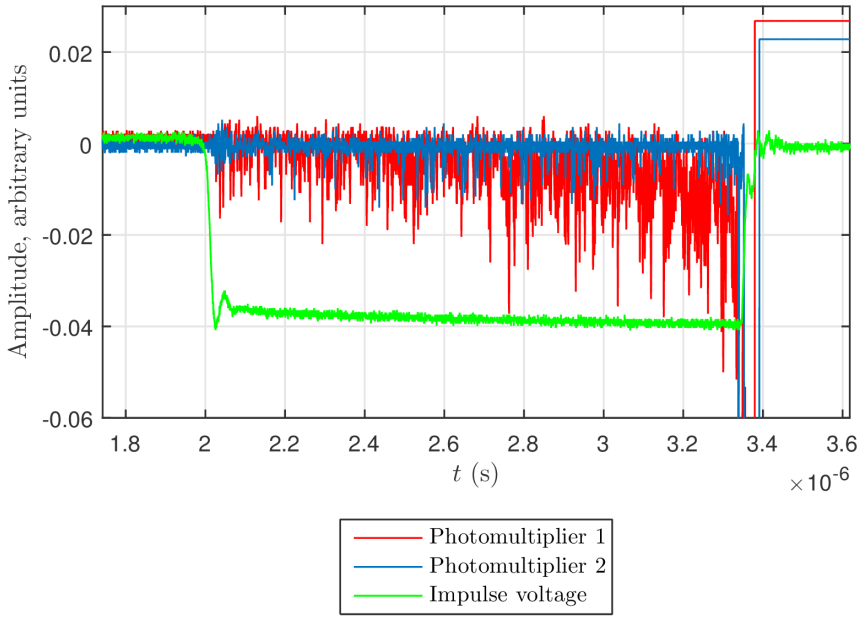

Figure 3.7: A typical plot of the the measured signals where the photomultiplier signals and the applied impulse voltage are measured as a function of time. A script is used to count the spikes of the two photomultiplier signals.

mainly defined manually by inspecting the recorded data. The script would then find all the local minima that are smaller than the defined limit.

Since the gap distance d can be measured, the average speed of streamers that managed to cross the gap can be calculated easily using a multiplot similar to the one in figure 3.7. After being triggered, the impulse voltage will set up a potential difference across the gap very quickly. This potential difference will be kept at a (more or less) constant level until it is set to zero after about 50 µs if the streamer does not bridge the gap during that time.

Conversely, if the streamer bridges the gap and causes a breakdown, the width of the impulse voltage would be narrower than 50 µs, which can be seen in figure 3.7. It is thus possible to determine which measurement recorded breakdown by inspecting the multiplots. The time that the streamer used to cross the gap can be found from the width of the impulse voltage, and the average speed can thus be calculated trivially.

3.2.3 Analysis of Onset Flares

For onset flares, a different approach was taken to analyze the data. The main measurement process was as mentioned in 3.2.1, but instead of performing eight measurements at various applied impulse voltages, 50 measurements were taken at the same voltage level. The applied impulse voltage was 50 kV for pure cyclohexane, and 60 kV for cyclohexane with pyrene.

After each experiment, the damaged glass, needle electrode and the test liquid was replaced with new units/samples, and the test cell was cleaned. The experiment was then repeated after changing parameters like the type of test liquid and optical filter.

Furthermore, the data analysis was mainly concerned with measuring the light amplitude and delay time as outlined in 2.3.

CHAPTER 4

Results and Discussion

In the first part of this chapter, the registered light from experiments performed in cyclohexane with pyrene is analyzed by using the two optical filters performing experiments with different configurations by changing parameters like the position of the needle and the needle point radius of the needle electrodes. The results are presented and discussed.

The results from the study of onset flares are given in the second part, where the correlation between the amplitude and delay time are discussed, as well as its behaviour in both pure cyclohexane and cyclohexane with pyrene.

4.1 Measurements of the Emitted Light at Various Levels of Applied Impulse Voltage

As explained in chapter 3, the emitted light were analyzed using two photomultipliers, where PM2 had an optical filter in front of it that filtered out part of the emitted light. The light transmitted by the optical filter and registered by PM2 was compared to the light registered by PM1. Only cyclohexane with pyrene was studied in the experiments presented in this section.

4.1.1 The Significance of the Needle Position

This subsection considers the effect that the needle position had on the emitted light. The needle was either placed in the bulk liquid or along the glass surface as illustrated in figure 4.1, and only needle electrodes with $r_p \sim 3\,\mu m$ were used. Figure 4.2 and 4.4 show the fraction N/N_0 of emitted light transmitted by the longpass filter as a function of the applied voltage, while figure 4.3 and 4.5 show the fraction of emitted light transmitted by the UV filter. Here and later, N and N_0 denote the number of spikes in the signals from PM2 and PM1 respectively.

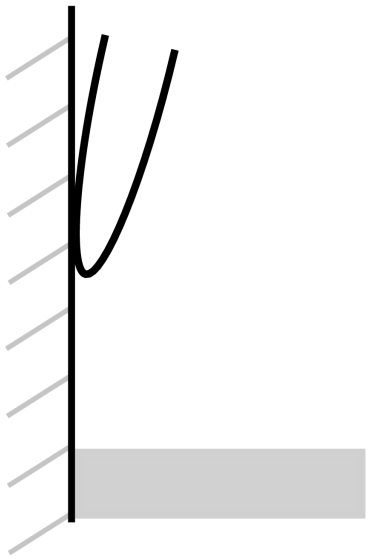

Figure 4.1: A needle electrode is placed along the glass surface. The grey area illustrates the plane electrode.

Figure 4.2 and 4.3 indicates that the fraction of UV light increases as the applied voltage is increased, while light with longer wavelengths seems to dominate at low voltages, and decreases as the applied impulse voltage increases. After reaching 45 kV, the fraction of emitted UV light and light with long wavelengths seems to reach an equilibrium. In this stage, these fractions appear to fluctuate around 10% and 40% respectively.

For experiments where the needle electrode was placed along the glass surface, a similar trend can be seen from figure 4.4 and 4.5. The most important difference compared to the cases where the needle was placed in the bulk liquid is the fraction of emitted UV light seems to be larger for almost every level of applied impulse voltage. Furthermore, the fraction of emitted light did not reach an equilibrium for the impulse voltage that was used. Instead, this fraction continued to increase with increasing V_{app}. These observations appear to be consistent with the hypothesis mentioned in 2.1.2, as the glass surface can

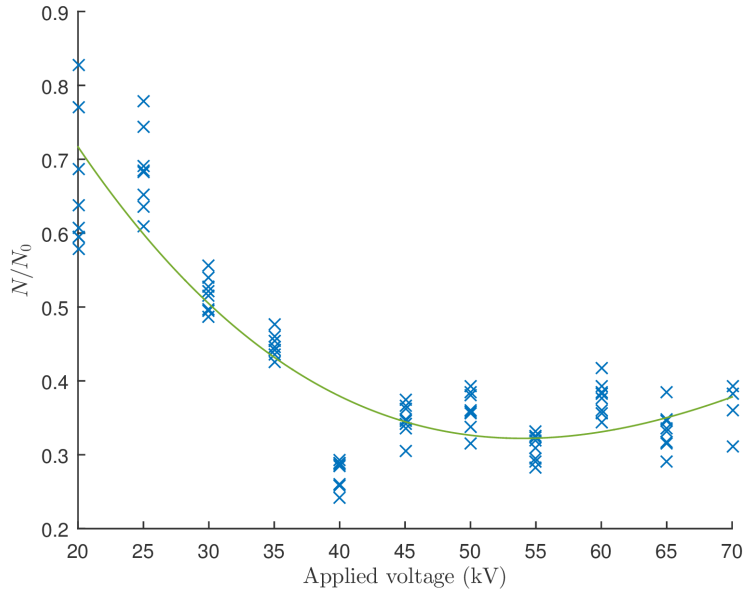

Figure 4.2: The fraction N/N_0 of light transmitted by the longpass filter as a function of applied voltage for a needle with $r_\mathrm{p} \sim 3\,\mu\mathrm{m}$ placed in the bulk liquid. N and N_0 denotes the number of spikes measured by PM2 and PM1 respectively. A trend line was added to the plot.

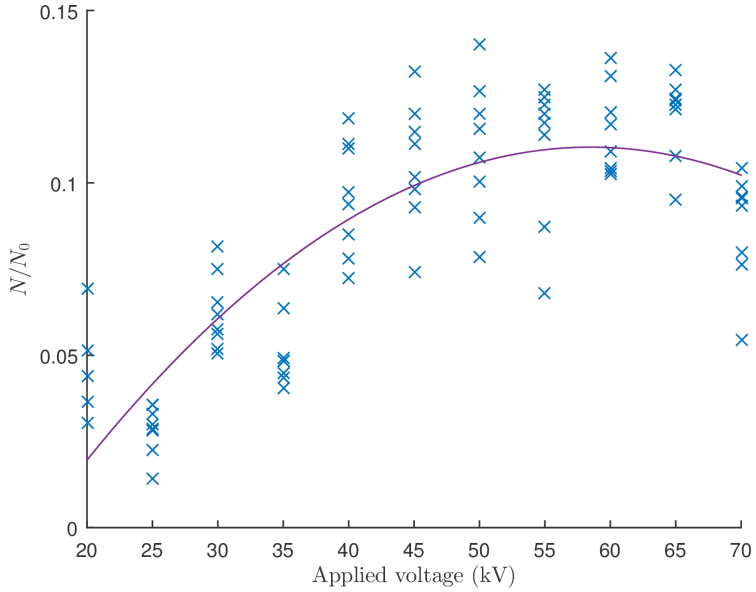

Figure 4.3: The fraction N/N_0 of emitted UV light as a function of applied voltage for a needle with $r_\mathrm{p} \sim 3\,\mu\mathrm{m}$ placed in the bulk liquid. N and N_0 denotes the number of spikes measured by PM2 and PM1 respectively. A trend line was added to the plot.

reduce the shielding effect so that the electric field around streamers is enhanced. The field enhancement can result in electrons with more kinetic energy, which can again initiate more luminous streamers. Hence, after removing roughly half of the shielding by

placing the needle electrode along a glass surface, more UV light can be emitted by the streamers.

Moreover, the increased strength of the tip field may explain why an equilibrium was not established when the needle electrode was placed along a glass surface. This suggest that the shielding effect contributes to the equilibrium seen in figure 4.3, which may be caused by the increasing degree of branching as V_{app} increases. As the degree of branching increases and reduces the tip field strength of the streamers, this may eventually balance out the contribution from an increasing V_{app}. Thus, for experiments performed with the needle electrode placed in the bulk liquid, the amount of emitted UV light will remain at a constant level when the equilibrium is established.

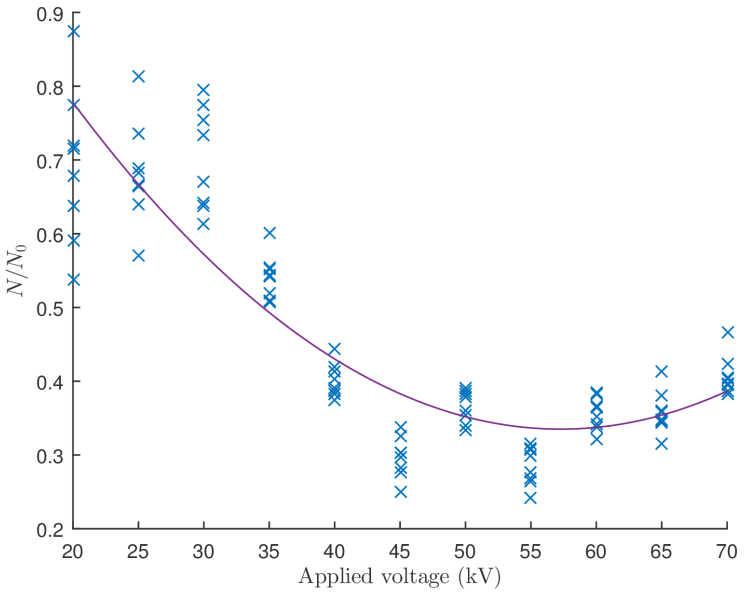

Figure 4.4: The fraction N/N_0 of light transmitted by the longpass filter as a function of applied voltage for a needle with $r_{\text{p}} \sim 3\,\mu\text{m}$ placed along a glass surface. N and N_0 denotes the number of spikes measured by PM2 and PM1 respectively. A trend line was added to the plot.

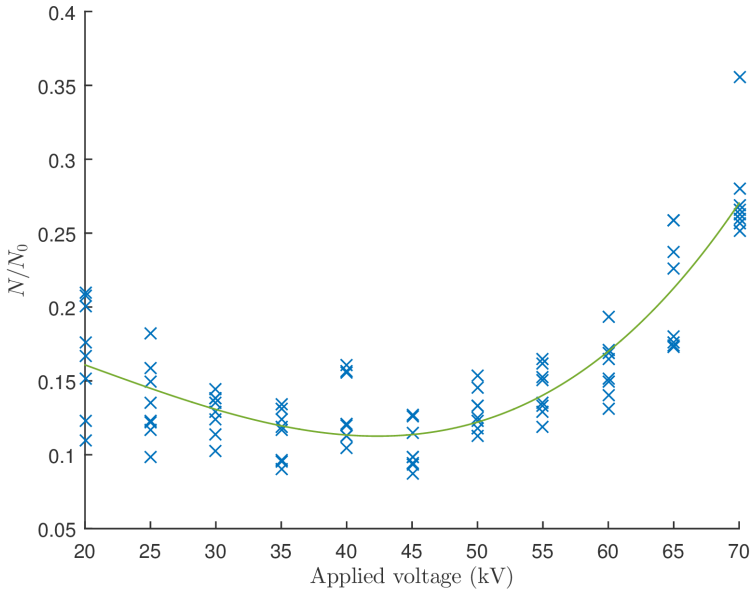

Figure 4.5: The fraction N/N_0 of emitted UV light as a function of applied voltage for a needle with $r_\mathrm{p} \sim 3\,\mu\mathrm{m}$ placed along a glass surface. N and N_0 denotes the number of spikes measured by PM2 and PM1 respectively. A trend line was added to the plot.

The average velocity for the observed streamers are plotted against applied voltage in 4.6. Results from both experiments where the needle electrode was placed in the bulk liquid and along a glass surface are plotted together. Both experiments used needle electrodes with $r_\mathrm{p} \sim 3\,\mu\mathrm{m}$, but had a slightly different gap distance due to the difficulty in positioning the needle electrode. The gap distance for the experiment with the needle electrode placed in the bulk liquid was 3.96 mm, while it was 3.47 mm for the other configuration.

As can be seen from figure 4.6, the average propagation velocity only depends weakly on the applied voltage, which agrees with earlier experiments. As mentioned in 2.1.1, it is known that the propagation velocity of second mode streamers only depends weakly on the applied voltage, while the number of filaments increases significantly with the applied voltage. Figure 4.6 clearly shows that the observed streamers propagated with an average velocity that belongs to the second mode, and is thus consistent with the proposed hypothesis regarding streamer branching and the equilibrium of the amount of emitted UV light mentioned above.

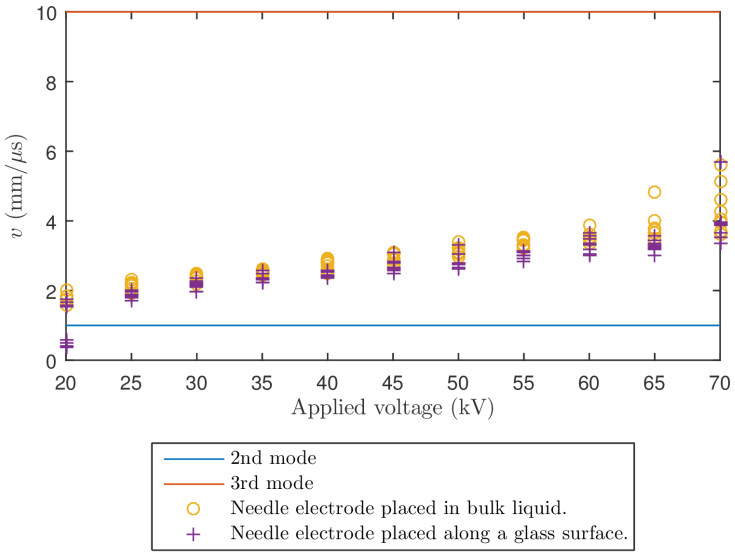

Figure 4.6: Average velocity for streamers observed in experiments using needle electrodes with $r_\mathrm{p} \sim 3\,\mu\mathrm{m}$ placed in the bulk liquid or along a glass surface. The gap distances in these two experiments were 3.96 mm and 3.47 mm respectively.

Furthermore, even though streamers propagating along a glass surface should have stronger tip fields due to the reduced shielding effect, they seem to propagate slower when compared to streamers that were propagating inside the bulk liquid. This may be caused by the absorption of free electrons and photons as mentioned in 2.1.2.

The largest source of error here comes from the measurement of the gap distance. However, this is still just $\sim 1\%$. Thus, a systematic error alone where one measurement series has been underestimated while the other has been overestimated cannot account for the difference in the velocities.

Both when the needle electrode was placed in the bulk liquid and along a glass surface, the fraction of emitted UV light increases with applied impulse voltage, while the opposite is true for the fraction of light transmitted by the longpass filter. In addition, since the average speed of streamers also increases with applied voltage, extrapolation of these observations suggest that photoionization may contribute significantly to streamer propagation for higher mode streamers.

4.1.2 The Significance of the Needle Point Radius

In this subsection, results from experiments using needles with point radii of $\sim 3\,\mu m$ and $\sim 15\,\mu m$ placed inside the bulk liquid are considered. The fraction of emitted light transmitted by the longpass and UV filters from experiments using needles with $r_p \sim 15\,\mu m$ are shown in figure 4.7 and 4.8 respectively.

Figure 4.7 shows that the fraction of light transmitted by the longpass filter decreases with increasing applied impulse voltage before reaching an equilibrium starting at $45 - 50\,kV$. This behaviour is similar to the case for a needle with $r_p \sim 3\,\mu m$, as shown in figure 4.2.

This is also true for the fraction of emitted UV light, as can be seen by comparing figure 4.3 and 4.8.

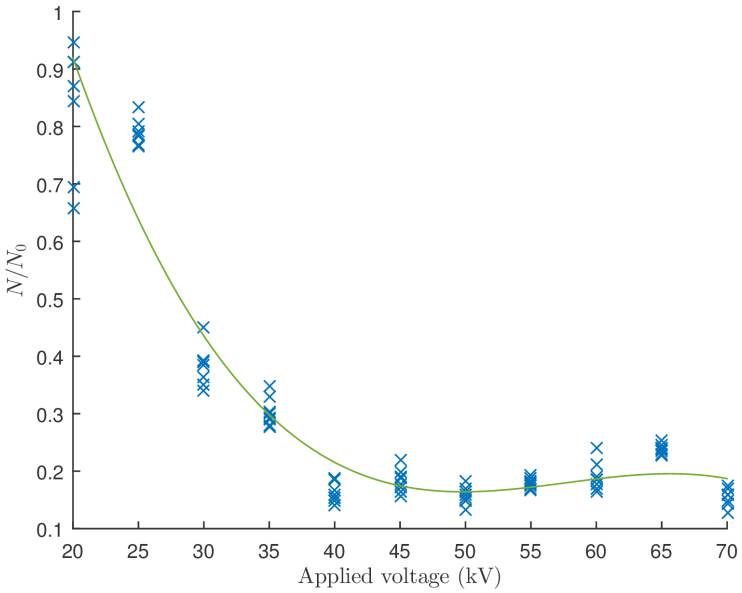

Figure 4.7: The fraction N/N_0 of light transmitted by the longpass filter as a function of applied voltage for a needle with point radius of $\sim 15\,\mu m$ placed inside the bulk liquid. N and N_0 denotes the number of spikes measured by PM2 and PM1 respectively. A trend line was added to the plot.

Finally, comparing figure 4.7 and 4.8, it can be seen that as in the case for a needle with $r_p \sim 3\,\mu m$, the first decreases with applied voltage, while the latter increases before both reaching an equilibrium around the same voltage. This observation is again a good indication that the streamers emit a significant fraction of light in the UV-range for high voltages, which is crucial for photoionization.

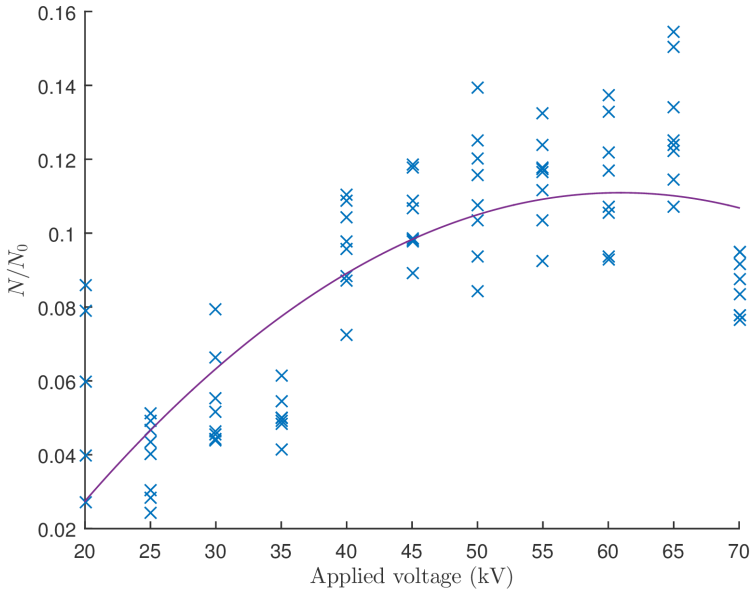

Figure 4.8: The fraction N/N_0 of emitted UV light as a function of applied voltage for a needle with point radius of $\sim 15\,\mu\text{m}$ placed inside the bulk liquid. N and N_0 denotes the number of spikes measured by PM2 and PM1 respectively. A trend line was added to the plot.

The corresponding velocity plot as a function of applied voltage is shown in figure 4.9. The average propagation speed again only weakly depends on the applied voltage, and the observed streamers seems to belong to the second mode. Thus, the results again display consistency with the proposed hypothesis regarding streamer branching and the equilibrium of the amount of emitted UV light mentioned above.

Streamers observed in experiments using needle electrodes with $r_\text{p} \sim 3\,\mu\text{m}$ are slightly faster at all voltage levels. Which is strange, since r_p should primarily be important for streamer inception. Again, a systematic error alone cannot account for this mismatch in velocity.

However, the bulk liquid will also act as an optical filter and absorb part of the UV light. Studies have shown that the photoabsorption cross section for cyclohexane is relatively large in the UV-range [18]. The photoabsorption cross section for cyclohexane is plotted against the wave length of the incident light in figure 4.10.

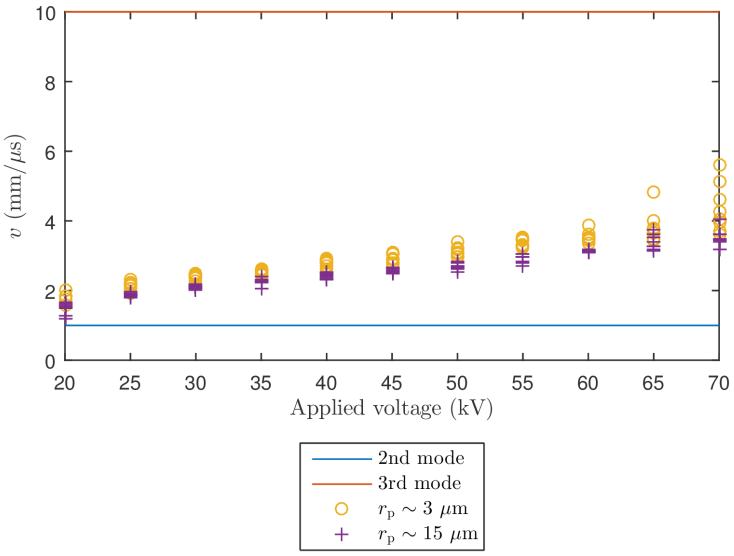

Figure 4.9: Average velocity for streamers observed in experiments using needle electrodes with $r_p \sim 3\,\mu m$ or $r_p \sim 15\,\mu m$ placed in the bulk liquid. The gap distances in these two experiments were 3.96 mm and 3.97 mm respectively.

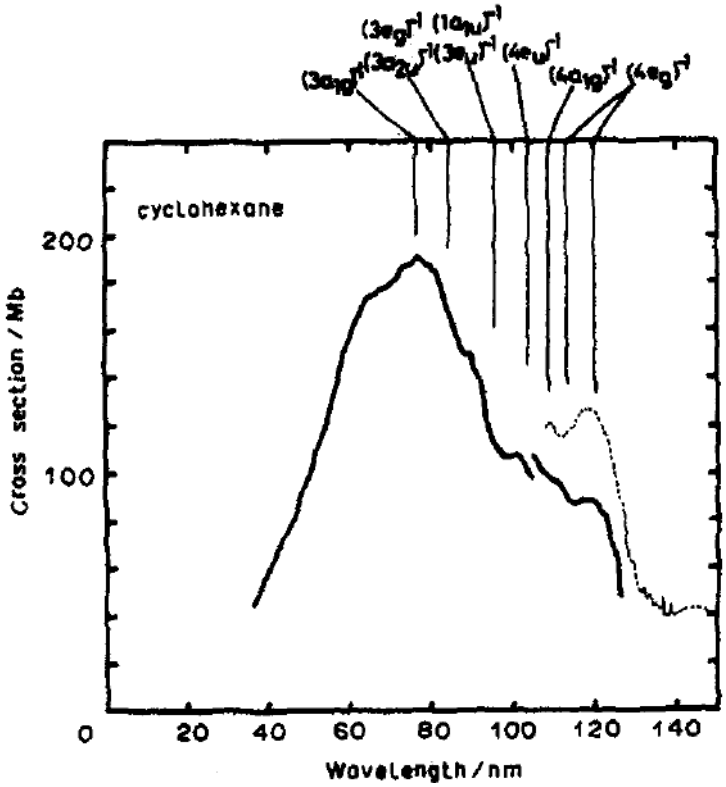

Figure 4.10: The photoabsorption cross section of cyclohexane V.S. the wavelength of incident photons. This figure was taken from [18]. The solid line is the results from [18], while the dashed line is results from [29]. The positions of ionic states are indicated [17].

Since cyclohexane will absorb part of the UV light, and this effect is largely removed when the needle electrode is placed along the glass surface, this may affect the statement that the fraction of emitted UV light seems to be larger when the needle electrode was placed along the glass surface compared to when it was placed in the bulk liquid.

Nevertheless, based on the same argument as in 4.1.1, these results also suggest that photoionization may contribute significantly to streamer propagation for higher mode streamers.

4.1.3 Uncertainties and Errors

First of all, performing measurements with different photomultipliers is a source of uncertainty. The method described in 3.2.2 assumes that both photomultipliers have roughly the same sensitivity for relevant wavelengths, but as mentioned in 3.1.2, the quantum efficiency is dependent on the wavelength of the incident photons and the cathode radiant sensitivity, which are different for the two photomultipliers. This will inevitably give rise to two kinds of uncertainty:

1. The dependence of wavelength may be a source of systematic errors and give a wrong picture of the relative amount of emitted light at different wavelengths.

2. Photomultipliers with different cathode radiant sensitivity may also be the source of systematic errors, since this can cause the photomultipliers to give different output signals even if they were measuring the same signal under the same conditions.

In addition to a difference in cathode radiant sensitivity, the photomultipliers also have different rise times. Since PM2 is more sensitive and has a shorter rise time than PM1, this can result in a larger fraction of transmitted light.

In order to compensate for the difference in sensitivity, an experiment was performed where the emitted light was measured at different voltage levels without any optical filters. The results indicate that PM2 registers roughly three times more light than PM1. Thus, the difference in sensitivity is compensated by letting $N/N_0 \rightarrow N/(3N_0)$. This compensation in sensitivity was however only based on one experiment, and may therefore not be very accurate. Ideally, measurements should be performed with the same type of photomultiplier.

The most crucial step in using the described method is to define suitable thresholds for counting the spikes. This was particularly difficult for high voltages when the amount of emitted light was large, and spikes could merge together. This may increase the fluctuations and represent a challenge in defining a proper threshold.

Given these uncertainties, the most accurate measurements should be those done at intermediate voltage levels, but even if the validity of the results are mainly restricted to intermediate voltages, the results still suggest that the amount of emitted UV light increases when the applied voltage increases. Since the higher mode streamers occurred at high voltages, the experiments indicate that photoionization is an important propagation mechanism for higher mode streamers.

4.1.4 Future Works

In order to relate the amount of emitted UV light to photoionization, it is important to study how much light is emitted by the streamer head itself. This setup can however only study the emitted light of the whole streamer including both streamer channel and streamer head.

A simple improvement can be made where narrow slits can be inserted in front of both photomultipliers. The lenses can be used to focus the emitted light into the slits, and thus it may be possible to distinguish between the light emitted by the streamer head and the streamer channel.

However, one should keep in mind that the emitted light may not be a continuous signal. Lesaint and Gournay [20] reported continuous signals in their experiments, which can be seen from figure 4.11. These experiments were performed with slower measuring devices[1], and showed that the current was mainly composed of continuous components.

Measurements from this thesis were however performed with faster equipments and results such as those shown in figure 4.12 indicates partially pulsed signals.

From figure 4.12, it can be seen that the signal from PM1 contains very few spikes at the beginning, but the number increases significantly towards the end (during the period $2 - 2.2\,\mu s$, there are about 7 spikes, while around 50 spikes are registered in the period

[1] A RTC 56AVP with anode pulse rise time 2 ns was used.

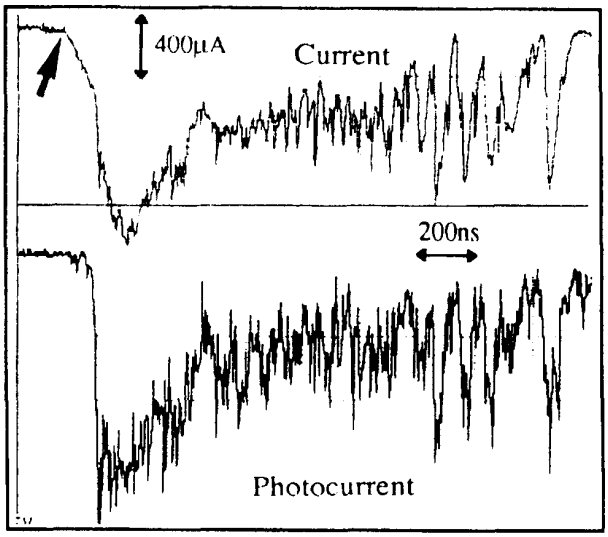

Figure 4.11: Current and photocurrent associated with the growth of a streamer propagating with velocity $> 1\,\mu m/ns$ in cyclohexane. The measurement was performed with $V_{app} = 20\,kV$, $d = 1.6\,mm$ and $r_p = 1.2\,\mu m$. The arrow indicates the onset of the applied voltage. This figure was taken from [20].

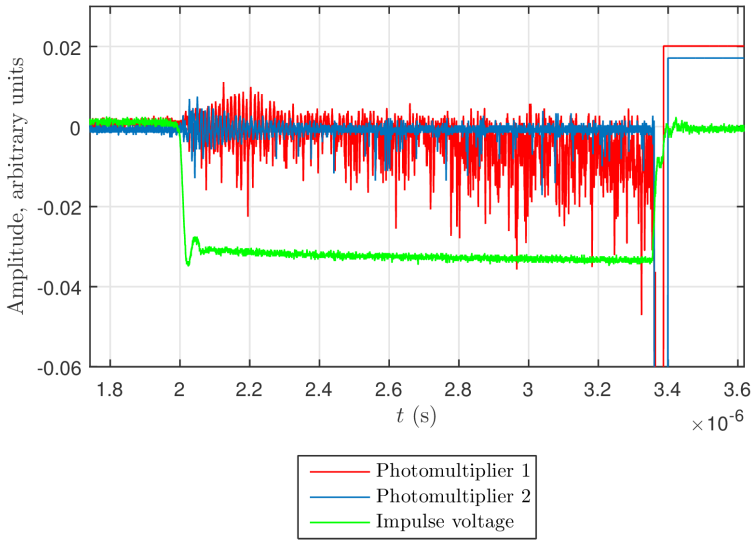

Figure 4.12: A plot of the recorded photomultiplier signals and probed voltage from an experiment performed with a needle with $r_p = 3\,\mu m$ placed in the bulk liquid (cyclohexane with pyrene). The applied voltage was 50 kV.

$3.1 - 3.3\,\mu s$). Moreover, it seems that the spikes at the beginning fall back to zero, while the spikes at the end do not, which may be caused by a superposition of several spikes. This indicates that a step-wise emission of light at the start of propagation, while the light emission towards the end may be continuous.

As mentioned in 2.1.1, it has been observed that plasma channels propagating in water have given rise to a series of discrete shock circles, which favours step propagation.

Part of the signal in 4.12 is enlarged and shown in figure 4.13. In this case, the time between two spikes in the beginning is of order $5 - 10\,\text{ns}$. From figure 4.9, it can be seen that streamers initiated at 50 kV have velocity $\sim 3\,\text{km/s}$. Thus, if the streamer has n braches at the time of interest, then the estimated stepsize is $15/n - 30/n$ µm.

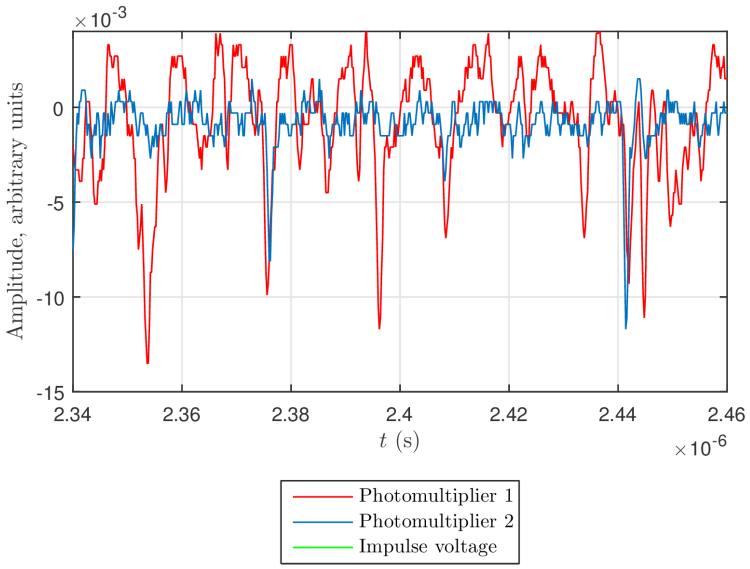

Figure 4.13: An enlarged version of part of the signal in figure 4.12.

However, even though the signals like that shown in figure 4.12 indicate step propagation because of its discrete spikes, one should be aware that a continuous signal may also be registered as discrete spikes if the amount of emitted light is small. I.e. if the amount of emitted light is small, then the discrete spikes may be caused by the registration of single photons. In order to distinguish between discrete spikes caused by a step propagation and registration of single photons, one can study the amplitude of dark currents in the photomultipliers. Box plots of the amplitude of dark currents of both photomultipliers as function of the photomultiplier voltage are shown in figure 3.4 and 3.5.

By studying the amplitudes at the relevant photomultiplier voltage (experiments in this thesis were carried out using 3 kV for PM1 and 4.5 kV for PM2.), and comparing to the amplitude of the discrete spikes, this may give an indication of whether the discrete spikes were truly caused by a step propagation or single photon pulses, since dark current pulses are probably caused by the registration of single photons. Simple comparison of results from an experiment performed with a needle electrode with $r_\text{p} \sim 15\,\mu\text{m}$ placed in

cyclohexane with pyrene, and without optical filters show that the amplitudes registered by PM1 are comparable to the largest dark current amplitudes at all V_{app}, while for PM2 this is only true at low V_{app}. For large values of V_{app}, most of the amplitudes in the PM2 signal are significantly larger than the dark current amplitudes. Thus, based on the signal from PM2, it seems that while measurements at low V_{app} cannot support step propagation, measurements at higher V_{app} indicate a step propagation (but only at the start of streamer propagation, when discrete pulses were registered).

Furthermore, results from this thesis can only give an indication of the contribution of photoionization to the propagation of higher mode streamers through extrapolation of the results. Future experiments should therefore aim to confirm this by studying the emitted light of higher mode streamers.

4.2 Measurement of Onset Flares

4.2.1 Experimental Results

As mentioned in 2.3, strong light impulses have been observed at high voltages. Results from [4] suggested that the ignition voltage for this phenomena lies somewhere between $39\,\text{kV} - 42\,\text{kV}$ for an experimental setup using needle electrodes with $r_{\text{p}} \sim 2\,\mu\text{m}$, gap distance $d \sim 4\,\text{mm}$ and pure cyclohexane with the needle electrode placed inside the bulk liquid. Furthermore, no correlation between applied impulse voltage and delay time was observed.

The experiments in this thesis used a similar setup where a needle electrode with $r_{\text{p}} \sim 3\,\mu\text{m}$ was placed inside the bulk liquid. The gap distance was $d \sim 4\,\text{mm}$, and the correlation between the light amplitude and the delay time was studied using different optical filters. The results for pure cyclohexane are given in figure 4.14-4.16.

As figure 4.14-4.16 indicates, there are no clear correlation between the amplitude and the delay time. However, as can be seen from these plots, the data points seem to be less scattered for large amplitudes. Furthermore, it seems that large amplitudes are less likely to occur early. From figure 4.15 it can also be seen that although not much UV light was registered for $50\,\text{kV}$, whenever the onset flare emitted UV light, $t_{\text{D}} > 12\,\text{ns}$.

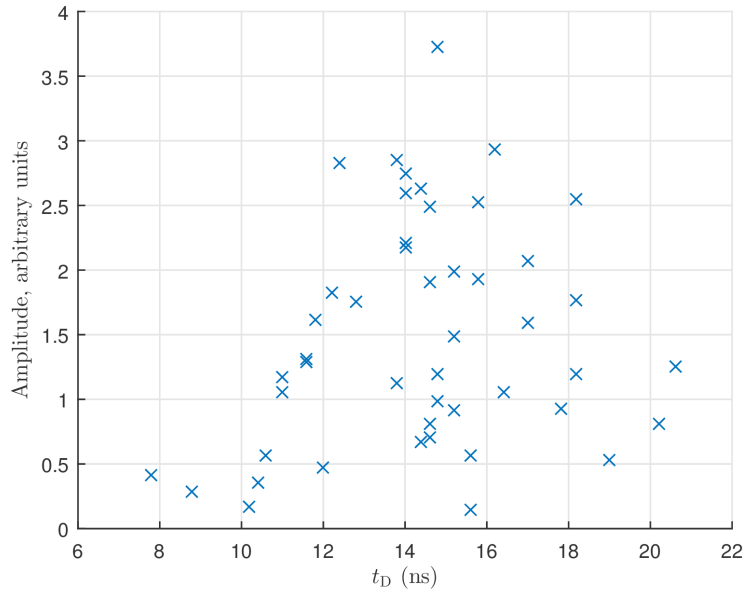

Figure 4.14: The light amplitude of registered onset flares plotted against the delay time t_D. These measurements were performed in pure cyclohecxane without any optical filters, and a needle electrode with $r_p \sim 3\,\mu m$ was placed in the bulk liquid.

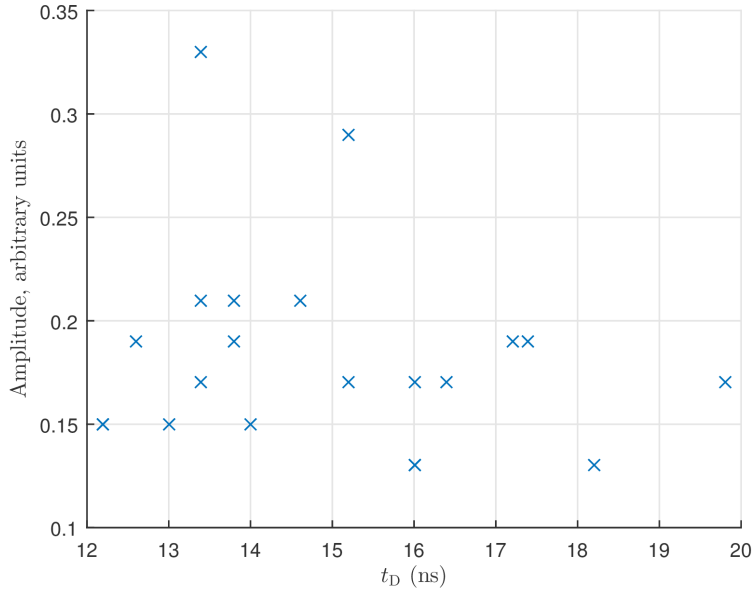

Figure 4.15: The light impulse amplitude plotted against the delay time t_D. These measurements were performed in pure cyclohecxane with an UV filter, and a needle electrode with $r_p \sim 3\,\mu m$ was placed in the bulk liquid.

The same measurements were repeated in cyclohexane with pyrene first using an impulse voltage of 70 kV and placing the needle electrode in the bulk liquid. However, the onset flares were rarely observed. 50 measurements were performed, but only four of them

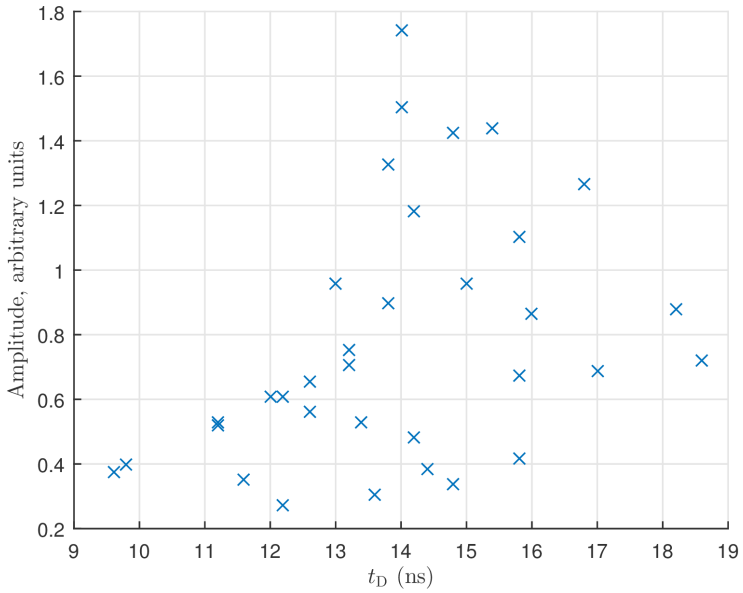

Figure 4.16: The light impulse amplitude plotted against the delay time t_D. These measurements were performed in pure cyclohecxane with a longpass filter, and a needle electrode with $r_p \sim 3\,\mu m$ was placed in the bulk liquid.

registered onset flares even though no optical filter was used.

Therefore, the needle electrode was along a glass surface instead, and the onset flares were observed already at 50 kV, and occurred close to 100% of the time at 60 kV. The same measurements were therefore repeated at 60 kV with the needle electrode placed along a glass surface. The results can be seen in 4.17-4.19.

It was initially theorized that onset flare may be caused by a large electron avalanche at streamer inception. If this is the case, then a large delay time should imply a larger stressed volume and hence a correspondingly large amplitude. Since the opposite has been observed in pyrene, another possible explanation is that a SCLF may be affecting the correlation between the light amplitude and delay time. I.e. a long delay time means a correspondingly reduced field, and thus a smaller amplitude.

The reason to why a similar behaviour was not observed in cyclohexane is not known. It seems like the effect of the SCLF is not sigificant at short t_D, and the long t_D observed in figure 4.17 and4.18 can either be caused by the additive or the glass surface. Thus, more experiment should be performed with the needle electrode placed along the glass surface in pure cyclohexane in order to distinguish whether this is caused by pyrene or the glass surface.

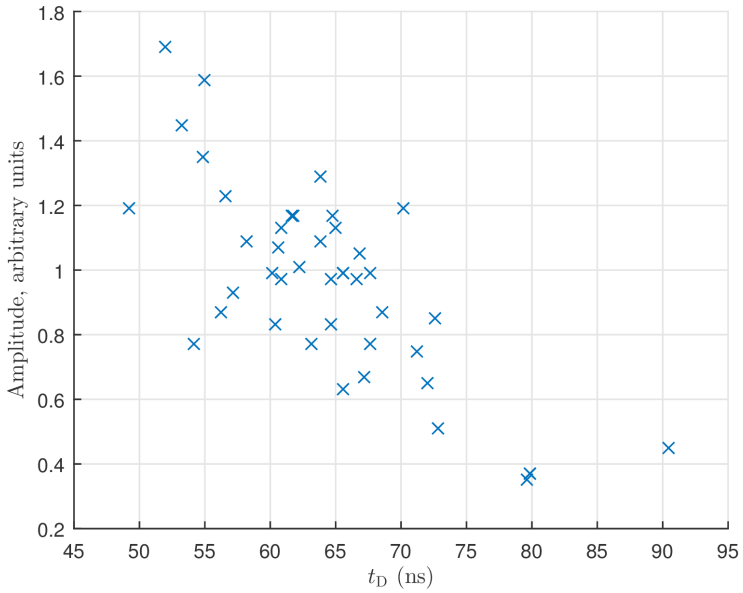

Figure 4.17: The light amplitude of registered onset flares plotted against the delay time t_D. These measurements were performed in cyclohexane with a 0.06 M concentration of pyrene without any optical filter and the needle electrode placed along a glass surface. $r_p \sim 3\,\mu m$.

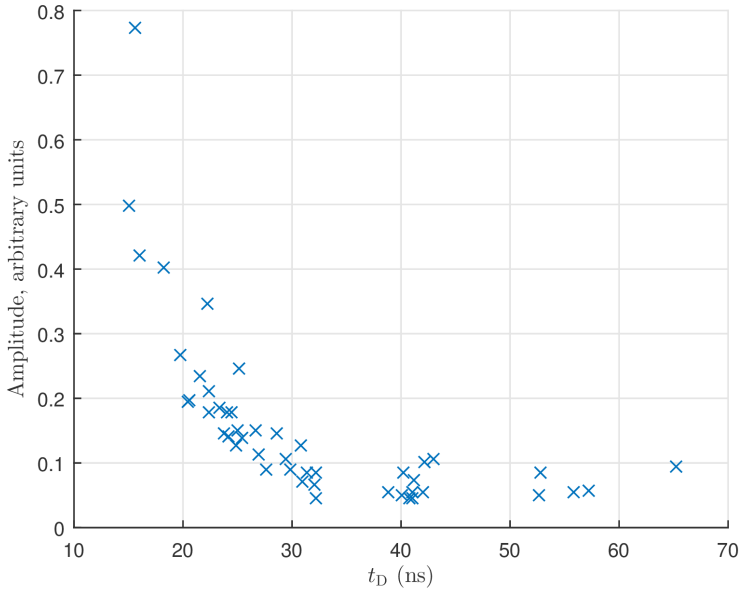

Figure 4.18: The light amplitude of registered onset flares plotted against the delay time t_D. These measurements were performed in cyclohexane with a 0.06 M concentration of pyrene and a UV filter. The needle electrode with $r_p \sim 3\,\mu m$ was placed along a glass surface.

As mentioned in 3.1.5, it has been observed that the addition of pyrene in cyclohexane will increase the acceleration voltage significantly, which may be explained by the shielding effect. Because of the decrease of the tip field, this may also have a similar effect on

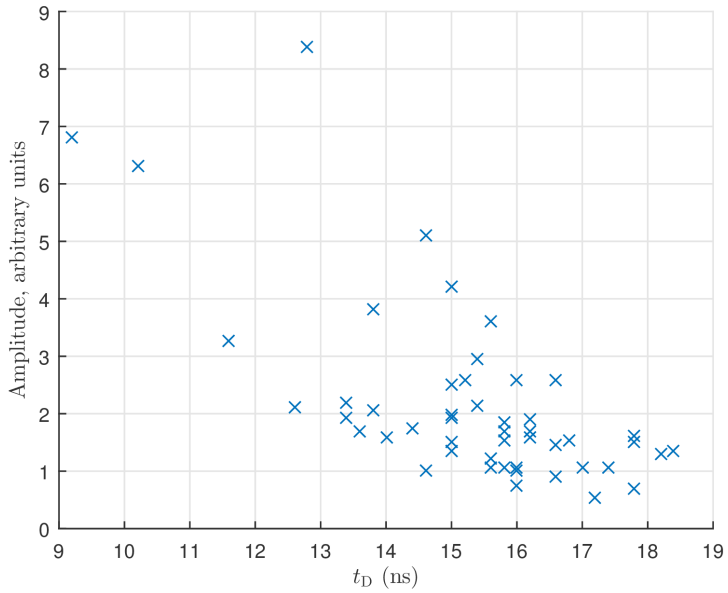

Figure 4.19: The light amplitude of registered onset flares plotted against the delay time t_D. These measurements were performed in cyclohexane with a 0.06 M concentration of pyrene and a longpass filter. The needle electrode with $r_p \sim 3\,\mu m$ was placed along a glass surface.

the occurrence of onset flares, such that higher voltages are required in order to initiate onset flares in cyclohexane with pyrene. On the other hand, placing the needle electrode along a glass surface would remove roughly half of the shielding effect due to streamer branching. This may explain why onset flares were observed steadily at a lower voltage when the needle electrode was placed along a glass surface compared to when it was placed in the bulk liquid.

However, a problem with this hypothesis is that onset flares mostly occur at the start of streamer propagation before significant branching should have been able to form. Thus, another possibility may be a similar decrease of shielding from the SCLF by placing the needle electrode along a glass surface. Furthermore, since the ionization potentials for pyrene and cyclohexane are very close to each other, this implies that an electron with sufficient energy to ionize cyclohexane, may also have enough energy to ionize pyrene. This may cause electron avalanches to build up faster and reduce the number of excited cyclohexane molecules compared to the case when only pure cyclohexane was used as the test liquid. Hence, if the light in the onset flares originated from excited cyclohexane molecules, this process will reduce the amount of available light that can cause an onset flare. Because of this increased efficiency in the buildup of charges, higher voltages may be required in order to initiate onset flares.

Furthermore, there is a significant mismatch in the axes of the plots in figures 4.17-4.19. Considering the fact that all these experiments were performed under similar conditions (components were replaced, and the test cell was cleaned between each experiment as described in 3.2.3), this may imply a systematic error in the measurements, especially since the amplitudes in figure 4.19 are even larger than those in figure 4.17[2]. Data from PM1 has been used as a control, which did not show any significant mismatch when compared to the corresponding PM2 signal. Thus, the error most likely did not originate from PM2. It was subsequently discovered that the measurements in 4.19 were not all independent, as outlined in 4.2.2. Although this is not able to directly explain the mismatch of the axes, it suggests that the data in 4.19 should be used with care, or even discarded.

4.2.2 Uncertainties, Errors and Future Works

Since this phenomenon has not been observed before, it was first suspected that this was not light that originated from inside the test cell. However, after removing the needle, this signal was not observed again regardless of the amplitude of the applied impulse voltage. Hence, this light impulse is linked to the streamers or the high field region created by the needle electrode.

As with the other experiments, the degradation of the test liquid may affect the results. As each measurement will further degrade the test liquid, this may have an impact on the amplitude of the later measurements.

Another parameter that was changed between measurements is the needle point radius. Successive breakdown will damage the needle electrode, and since needle electrodes with very small point radii were used, this damage is significant, as can be seen from figure 4.20 and figure 4.21.

Figure 4.20 and 4.21 depict the same needle electrode before and after an experiment. Clearly, the point radius has changed significantly before and after use. The electric field E_1 and E_2 at the needle tip before and after use can be compared by using equation (3.2). Inserting the corresponding numerical values yields $E_1 \approx 5E_2$. This may explain why

[2]Since the data in figure 4.19 was measured with an optical filter, while the data in figure 4.17 was measured without an optical filter, the light amplitude in figure 4.17 should not be larger than those in figure 4.17

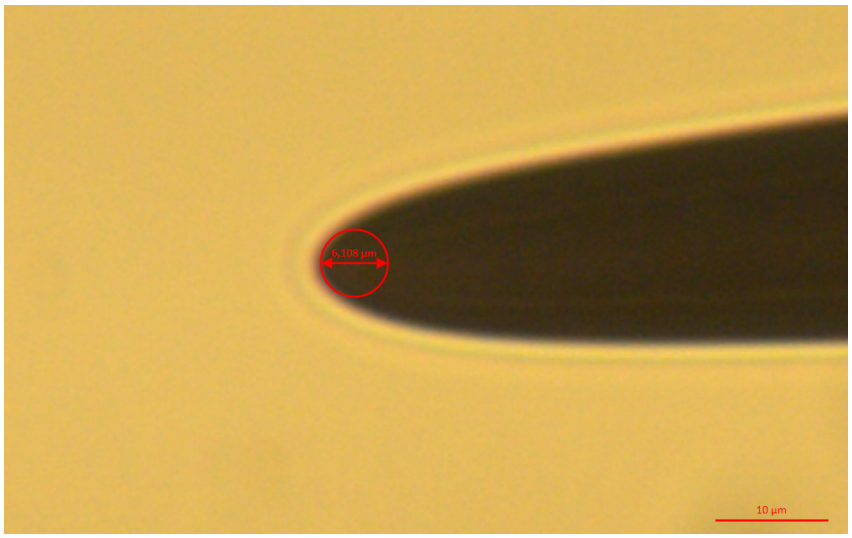

Figure 4.20: Picture of one of the needle electrodes before use. $r_\mathrm{p} \approx 3\,\mu\mathrm{m}$.

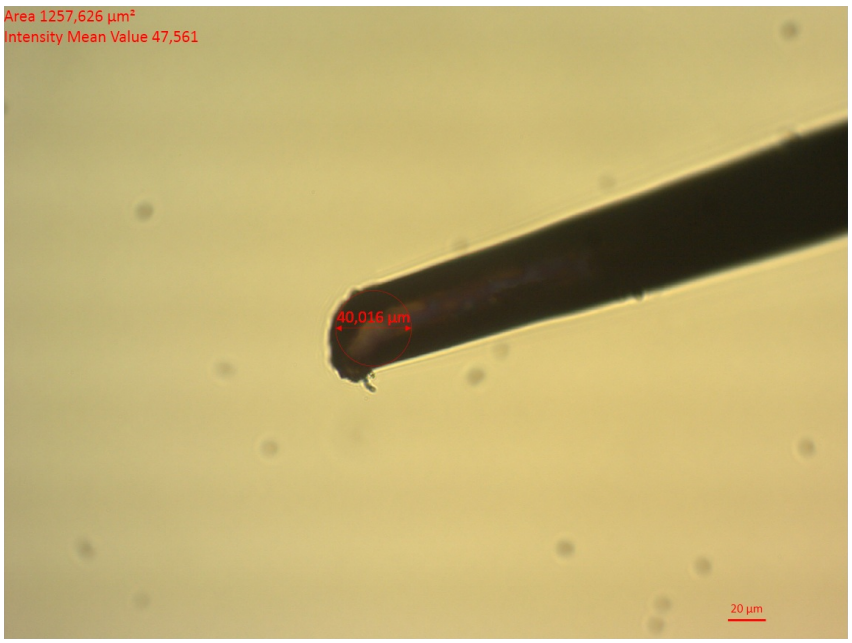

Figure 4.21: Picture of the needle electrode in figure 4.20 after use. $r_\mathrm{p} \approx 20\,\mu\mathrm{m}$.

more onset flares with small amplitudes were observed. If this damage is significant, the light amplitude should be decreasing between measurements. However, this not true in all experiments, as shown in figure 4.22 and figure 4.24, where the light amplitude is plotted against the number of measurement. In experiments performed with the needle electrode inside the bulk liquid, a decreasing trend is non-existing, with results similar to those given in figure 4.22. For experiments performed with the needle electrode along a glass surface, a weak decreasing trend can be seen like in figure 4.23, but the measurements can still be regarded as independent of each other.

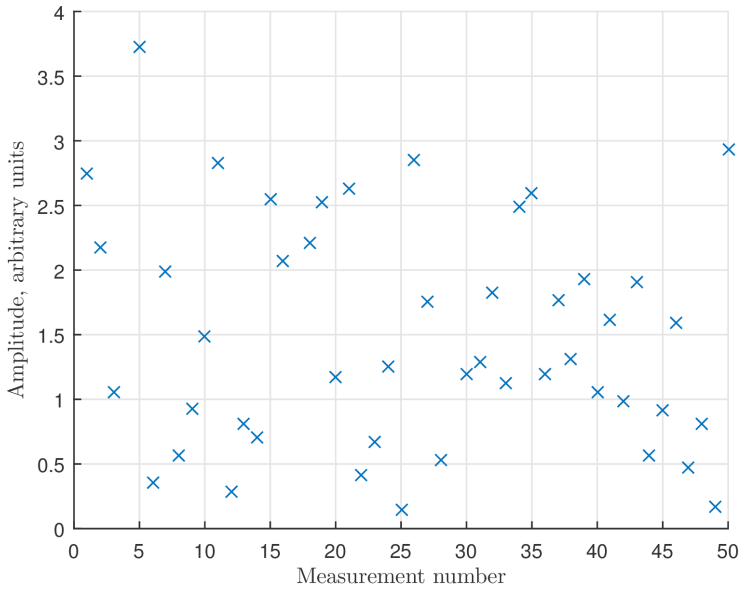

Figure 4.22: A plot of the light amplitude against measurement number for an experiment performed in cyclohexane. No optical filter was used, and the needle electrode with $r_{\mathrm{p}} \sim 3\,\mu\mathrm{m}$ was placed in the bulk liquid. The data is from the same experiment as figure 4.14.

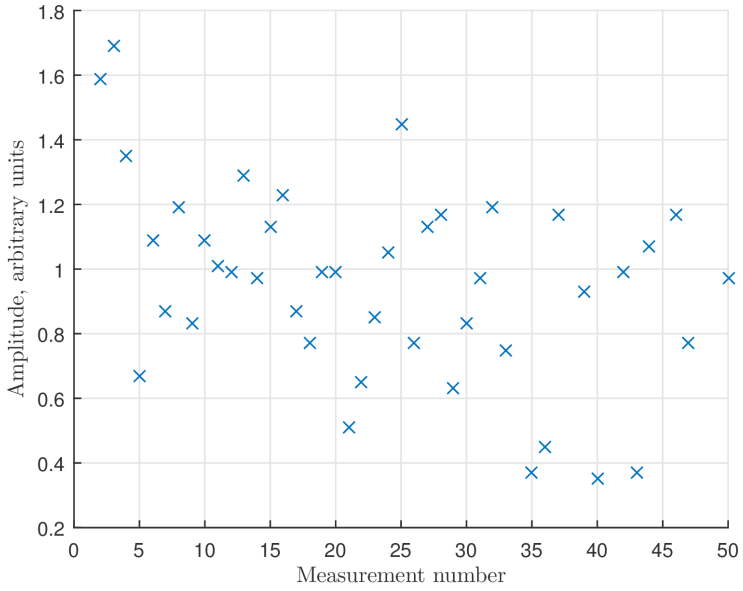

Figure 4.23: A plot of the light amplitude against measurement number for an experiment performed in cyclohexane with pyrene. No optical filter was used, and the needle electrode with $r_{\mathrm{p}} \sim 3\,\mu\mathrm{m}$ was placed along a glass surface. The data is from the same experiment as figure 4.17.

However, when data corresponding to those shown in figure 4.19 were analysed in the same manner, a strong decreasing behaviour can be seen, as shown in figure 4.24. Thus, the

data shown in figure 4.19 should be used with care, as this indicates a strong dependence between succesive measurements.

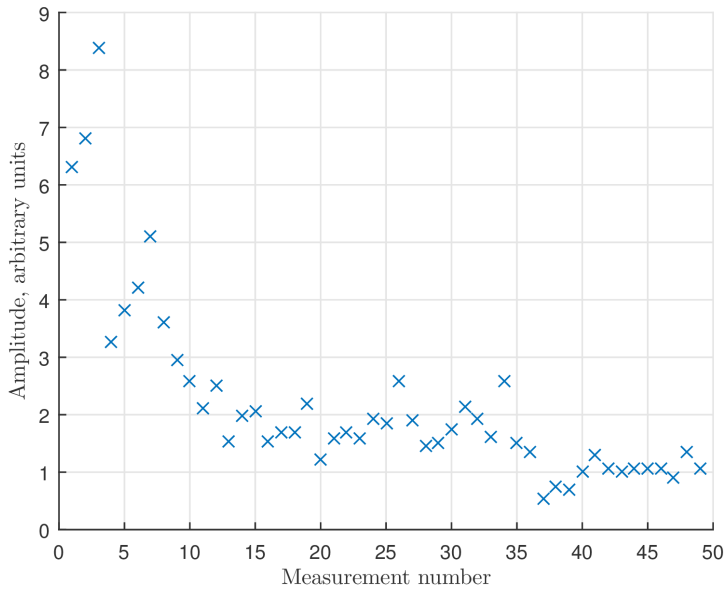

Figure 4.24: A plot of the light amplitude against measurement number for an experiment performed in cyclohexane with pyrene. The longpass filter was used, and the needle electrode with $r_\mathrm{p} \sim 3\,\mu\mathrm{m}$ was placed along a glass surface. The data is from the same experiment as figure 4.19.

Another possible explanation for this observation, in addition to the damaged needle, glass and test liquid, is that some of the charges may have been clinging to the glass surface, and the waiting time between each measurements was not sufficient for the charges to diffuse away from the surface. In the bulk liquid, it may have been easier for free charges to diffuse away, but in the presence of a solid surface, the opportunities for diffusion is reduced. Thus, the surface charge density may have increased as the number of measurements and breakdowns increased and caused an increasing distortion to the electric field as described by equation (2.3). It is however difficult to study this distortion properly without knowledge of σ_f, but for future work, it may be useful to use test liquids with different ε_r in order to study the effect this may have on onset flares.

For unknown reasons, this effect seems to have been highly significant in the experiment corresponding to figure 4.19, but less significant for the other experiments where the needle electrode was placed along a glass surface. This may have been caused by random experimental mistakes such as not properly cleaned glass. This situation can possibly be avoided by increasing the waiting time between measurements in order to give free charges sufficient time to diffuse away from the glass surface.

Other future works that can be considered in order to study the various statements mentioned in 4.2.1 are

1. using molecular dynamics simulation to simulate electron avalanches in cyclohexane with pyrene in order to investigate whether pyrene truly can suppress onset flares by improving the efficiency of electron avalanches as mentioned in 4.2.1.

2. measuring the electric field using for instance a two dimensional Kerr measurement system [11] in order to study how SCLF may affect the amplitude and delay time of onset flares. However, the sensitivity of the Kerr method is low for non-polar liquids, and low spatial and temporal resolution represent significant challenges.

3. In addition to studying onset flares in pure cyclohexane along a glass surface as mentioned in 4.2.1, the significance of the surface material should also be studied by placing the needle electrode along various materials that are transparent in the UV region.

CHAPTER 5

Conclusion

Photoionization has been proposed as an important propagation mechanism that enhances the propagation of higher mode streamers, since studies have shown that electron mobility is too low to explain the velocity of higher mode streamers. In order for photoionization to be a major propagation mechanism, a large fraction of the emitted light should be UV light.

Despite the uncertainties, the experiments performed in this thesis work were able to qualitatively show that the amount of UV light emitted both by streamers propagating in cyclohexane and cyclohexane with dissolved pyrene increased with applied voltage, while the opposite was observed for light with long wavelength. In some cases, after a certain applied voltage was reached, the fraction of emitted UV light seemed to remain at a constant level for the rest of the experiment. It is suggested that this is due to the fact that most streamers observed in these experiments seemed to be second mode streamers, and that the number of filaments for second mode streamers increases significantly with applied voltage, and may thus induce an electric shielding effect.

Overall, extrapolation of the results suggests that photoionization may indeed be important for propagation of higher mode streamers. However, this has to be further studied by studying the emitted light from higher mode streamers. Moreover, the emitted light from the streamer heads should be studied, but results from this thesis work indicate that the observed streamers may have a partially stepped propagation, which represents a challenge for studies focused on studying the emitted light from the streamer heads.

Powerful light impulses dubbed onset flares in this thesis work have been observed at the onset of streamer formations under certain conditions, which have not been previously reported. The correlation between light amplitude and delay time was studied in order to investigate possible mechanisms responsible for such pulses. In some of the experiments, it was found that the light amplitude decreased with delay time, and SCLFs have been proposed as an important factor for causing this behaviour. In experiments where this was not observed, another mechanism that links a long delay time to a larger stressed volume, and thus a larger electron avalanche and light amplitude is believed to also contribute. In order to study how SCLF may affect the light amplitude and delay time, a two dimensional Kerr measurement system may be useful.

Furthermore, it was found that it is more difficult to initiate onset flares in cyclohexane with pyrene than pure cyclohexane. The suggested cause for this behaviour is due to more efficient charge buildups and electron avalanches after addition of pyrene, which has a very similar ionization potential compared to cyclohexane. The increased efficiency in electron avalanches may be so significant that the number of excited molecules that may emit light does not become significant until a higher voltage is reached. This should however be further studied, and one possible method is by using molecular dynamics simulation.

Bibliography

[1] V. M. Atrazhev, V. S. Vorob'ev, I. V. Timoshkin, M. J. Given, and S. J. MacGregor. Mechanisms of impulse breakdown in liquid: The role of joule heating and formation of gas cavities. *IEEE Transactions on Plasma Science*, 38(10):2644–2651, 2010.

[2] P. Ceccato. *Filamentary plasma discharge inside water : initiation and propagation of a plasma in a dense medium*. Phd theses, Ecole Polytechnique X, December 2009.

[3] P. H. Ceccato, O. Guaitella, M. Rabec Le Gloahec, and A. Rousseau. Time-resolved nanosecond imaging of the propagation of a corona-like plasma discharge in water at positive applied voltage polarity. *Journal of Physics D: Applied Physics*, 43(17):175202, 2010.

[4] J. B. B. Chen. Light Emission of Streamers in Dielectric Liquid. Specialization Project, Norwegian University of Science and Technology, 2016. Unpublished.

[5] L. G. Christophorou. *Atomic and Molecular Radiation Physics*. Wiley Monographs in Chemical Physics. John Wiley & Sons Canada, Limited, 1971.

[6] R. Coelho and J. Debeau. Properties of the tip-plane configuration. *Journal of Physics D: Applied Physics*, 4(9):1266, 1971.

[7] N. Davari. *Molecular modeling of ionization processes relevant for electrically insulating liquids*. PhD thesis, Norwegian University of Science and Technology, Trondheim, 2015.

[8] N. Davari, P.-O. Åstrand, M. Unge, L. E. Lundgaard, and D. Linhjell. Field-

dependent molecular ionization and excitation energies: Implications for electrically insulating liquids. *AIP Advances*, 4(3):7117, 2014.

[9] A. Denat, J. P. Gosse, and B. Gosse. Electrical conduction of purified cyclohexane in a divergent electric field. *IEEE Transactions on Electrical Insulation*, 23(4):545–554, Aug 1988.

[10] L. Dumitrescu, O. Lesaint, N. Bonifaci, A. Denat, and P. Notingher. Study of streamer inception in cyclohexane with a sensitive charge measurement technique under impulse voltage. *Journal of Electrostatics*, 53(2):135 – 146, 2001.

[11] U. Gafvert. Two dimensional measurements of electrical fields in transformer oil. In *Annual Conference on Electrical Insulation and Dielectric Phenomena*, pages 667–671, Oct 1990.

[12] P. Gournay and O. Lesaint. A study of the inception of positive streamers in cyclohexane and pentane. *Journal of Physics D: Applied Physics*, 26(11):1966, 1993.

[13] P. Gournay and O. Lesaint. On the gaseous nature of positive filamentary streamers in hydrocarbon liquids. ii: Propagation, growth and collapse of gaseous filaments in pentane. *Journal of Physics D: Applied Physics*, 27(10):2117, 1994.

[14] R. E. Hebner. *Measurement of Electrical Breakdown in Liquids*, pages 519–537. Springer US, Boston, MA, 1988.

[15] Ø. L. G. Hestad. *Prebreakdown phenomena in solids and liquids stressed by fast transients: The effect of additives and phase.* PhD thesis, Norwegian University of Science and Technology, Trondheim, 2010.

[16] R. E. Jorgenson, L. K. Warne, A. A. Neuber, J. Krile, J. Dickens, and H. Krompholz. *Effect of dielectric photoemission on surface breakdown: An LDRD report.* 2003.

[17] M. Kimura and K. Lacmann. Energy and angular differential cross sections for K + NO_2 charge transfer reactions. *Chemical Physics Letters*, 70(1):41 – 44, 1980.

[18] H. Koizumi, K. Shinsaka, and Y. Hatano. VUV-optical oscillator strength distributions of molecules and their implications to early events in radiation chemistry.

Radiation Physics and Chemistry, 34:87–92, 1989.

[19] O. Lesaint. Prebreakdown phenomena in liquids: propagation 'modes' and basic physical properties. *Journal of Physics D: Applied Physics*, 49(14):144001, 2016.

[20] O. Lesaint and P. Gournay. Initiation and propagation thresholds of positive prebreakdown phenomena in hydrocarbon liquids. *IEEE Transactions on Dielectrics and Electrical Insulation*, 1(4):702–708, Aug 1994.

[21] O Lesaint and M Jung. On the relationship between streamer branching and propagation in liquids: influence of pyrene in cyclohexane. *Journal of Physics D: Applied Physics*, 33(11):1360, 2000.

[22] O. Lesaint and G. Massala. Transition to fast streamers in mineral oil in the presence of insulating solids. In *Conference Record of the 1996 IEEE International Symposium on Electrical Insulation*, volume 2, pages 737–740 vol.2, 1996.

[23] O. Lesaint and G. Massala. Positive streamer propagation in large oil gaps: experimental characterization of propagation modes. *IEEE Transactions on Dielectrics and Electrical Insulation*, 5(3):360–370, Jun 1998.

[24] T. J. Lewis. A new model for the primary process of electrical breakdown in liquids. *IEEE Transactions on Dielectrics and Electrical Insulation*, 5(3):306–315, 1998.

[25] P. F. Little. *Secondary Effects*, pages 574–663. Springer-Verlag Berlin Heidelberg, 1956.

[26] L. Lundgaard, D. Linhjell, G. Berg, and S. Sigmond. Propagation of positive and negative streamers in oil with and without pressboard interfaces. *IEEE Transactions on Dielectrics and Electrical Insulation*, 5(3):388–395, Jun 1998.

[27] I. Madshaven, H. S. Smalø, M. Unge, and Ø. L. G. Hestad. Photoionization model for the transition to fast mode streamers in dielectric liquids. *Unpublished*.

[28] A. Messiah. *Quantum Mechanics*. Mineola: Dover Publications, Inc., 2014.

[29] J. W. Raymonda and W. T. Simpson. Experimental and theoretical study of sigma-

bond electronic transitions in alkanes. *The Journal of Chemical Physics*, 47(2):430–448, 1967.

[30] W. F. Schmidt. *Liquid State Electronics of Insulating Liquids*. CRC Press LLC, 1997.

[31] H. S. Smalø, Ø. L. G. Hestad, S. Ingebrigtsen, and P.-O. Åstrand. Field dependence on the molecular ionization potential and excitation energies compared to conductivity models for insulation materials at high electric fields. *Journal of Applied Physics*, 109(7):073306, 2011.

[32] H. Sueda and K. C. Kao. Prebreakdown phenomena in high-viscosity dielectric liquids. *IEEE Transactions on Electrical Insulation*, EI-17(3):221–227, 1982.

APPENDIX A

Townsend Mechanism

A positive Townsend discharge is initiated by a seed electron close to the anode, which is created through a stochastic ionization process of a molecule. This "seed ionization" can be caused by processes such as cosmic background radiation [30] and thermal inelastic collisions between molecules.

The seed electron will then be accelerated towards the anode, while the positive ion will be left quasi-stationary and act as an extension of the electric potential of the streamer. This acceleration will increase the kinetic energy of the electron until it collides with another atom/molecule. There are then five possible outcomes:

1. The molecule is ionized through impact ionization, which liberates one or more additional electrons.

2. The electron transfers part of its energy to excite the molecule.

3. A combination of outcome 1 and 2.

4. Elastic collision that only changes the direction of motion.

5. The electron is absorbed by the molecule and results in a negative ion.

For sufficiently large mean free path ℓ, the electrons will gain enough energy between

collisions for the first and third outcome to dominate. If a collision between the electron and the atom/molecule X yields n additional electrons, this process can be written as

$$X + e^- \rightarrow X^{n+} + (n+1)e^-. \tag{A.1}$$

This will result in a chain reaction called an electron avalanche that generates a large amount of free electrons.

In kinetic gas theory, the mean free path of a particle being launched at an ensemble of identical target particles is given by

$$\ell = \frac{1}{n\sigma}, \tag{A.2}$$

where n [1] is the number density of target particles and σ is the scattering cross section of a target particle.

If the velocities of the target particles has a Maxwell-Boltzmann distribution, equation (A.2) is modified by a factor $1/\sqrt{2}$:

$$\ell = \frac{1}{\sqrt{2}n\sigma}. \tag{A.3}$$

Assuming that the ensemble of target particles behaves similar to an ideal gas, the number density is given by

$$n = \frac{N}{V} = \frac{p}{k_\mathrm{B}T}. \tag{A.4}$$

Let μ be the mass of a target particle. The total mass mass of the ensemble of target particles is then $M = N\mu$. Combined with equation (A.4), this yields

$$n = \frac{\rho}{\mu}, \tag{A.5}$$

where ρ is the mass density of the ensemble of target particles.

Furthermore, assuming that the target particles can be approximated as hard spheres with radius r, the scattering cross section is simply the cross section area of such a sphere, i.e.

$$\sigma = 4\pi r^2. \tag{A.6}$$

[1] Not to be confused with n used in the reaction equation (A.1).

Inserting equation (A.5) and (A.6) into equation (A.3) yields

$$\ell = \frac{\mu}{4\sqrt{2}\pi r^2 \rho}. \tag{A.7}$$

Townsend's first ionization coefficient α is defined as the probability for a collision per unit length in the field direction to ionize the target molecule. It can therefore be written as

$$\alpha = N_{\mathrm{c}} P_{\mathrm{i}}, \tag{A.8}$$

where N_{c} is the number of collisions between an electron and molecules per unit length in the direction of the electric field and P_{i} is the probability for a collision to ionize the target molecule.

P_{i} increases with the accumulated kinetic energy of the electrons. Since the acceleration is proportional to the electric field strength E, and the relation between final velocity v, acceleration a and acceleration distance s can be approximated[2] as $v^2 = 2as$, the kinetic energy E_{k} can be written as

$$E_{\mathrm{k}} \sim E\ell. \tag{A.9}$$

Furthermore, equation (A.7) states that $\ell \sim 1/\rho$. The probability probability for a collision to ionize the target molecule should therefore be a function of E/ρ.

The number of collisions N_{c} is proportional to the number density of target particles, which is again proportional to the mass density ρ. Thus, Townsend's first ionization coefficient is density dependent, and can be written as

$$\alpha = f\left(\frac{E}{\rho}\right)\rho. \tag{A.10}$$

[2]Assuming approximately linear motion between collisions with constant acceleration.

Index